

Supplementary Materials for

**Exceeding Flexpectations: A Combined Experimental and Computational Investigation of Structural Flexibility in 3-Dimensional Linker-Based Metal-Organic Frameworks**

Courtney S. Smoljan<sup>1</sup>, Filip Formalik<sup>1,2</sup>, Michael L. Barsoum<sup>3,†</sup>, Kira M. Fahy<sup>4,†</sup>, Madeleine A. Gaidimas<sup>4,†</sup>, Florencia A. Son<sup>4,†</sup>, Haomiao Xie<sup>4</sup>, Karam B. Idrees<sup>4</sup>, Omar K. Farha<sup>1,4,\*</sup>, Randall Q. Snurr<sup>1,\*</sup>

<sup>1</sup>*Department of Chemical and Biological Engineering, Northwestern University, Evanston, IL 60208, United States*

<sup>2</sup>*Department of Micro, Nano, and Bioprocess Engineering, Faculty of Chemistry, Wroclaw University of Science and Technology, Wroclaw 50-370, Poland*

<sup>3</sup>*Department of Materials Science and Engineering, Northwestern University, Evanston, IL 60208, United States*

<sup>4</sup>*Department of Chemistry and International Institute for Nanotechnology, Northwestern University, Evanston, IL 60208, United States*

<sup>†</sup>*These authors contributed equally.*

\*Correspondence: Omar K. Farha – [o-farha@northwestern.edu](mailto:o-farha@northwestern.edu); Randall Q. Snurr – [snurr@northwestern.edu](mailto:snurr@northwestern.edu)

## Contents

1. Experimental Methods .....	3
1.1 Material Synthesis and Preparation .....	3
1.1.1 Single Crystals of NU-2003 .....	3
1.1.2 Material Synthesis and Preparation for Compression Experiments .....	3
1.2 Material Characterization.....	3
1.2.1 Powder X-ray Diffraction Under Ambient Conditions .....	3
1.2.2 Single Crystal X-ray Diffraction Experiment for NU-2003 .....	3
1.3 In Situ Variable Pressure X-ray Diffraction Experiments .....	4
1.3.1 Experimental Setup.....	4
1.3.2 Refinement Details.....	4
1.3.3 Bulk Modulus Calculation.....	4
2. Computational Methods .....	5
2.1 Density Functional Theory (DFT) Geometry Optimizations .....	5
2.2 Young's Moduli Calculations .....	7
2.3 Grand Canonical Monte Carlo Simulations .....	8
3. Supplemental Text and Additional Results .....	9
3.1 Material Characterization.....	9
3.1.1 Powder X-ray Diffraction under Ambient Conditions .....	9
3.1.2 Crystallographic Information for NU-2003 .....	11
3.2 Computational Results .....	13
3.2.1 Optimized Condensed Phases from DFT Calculations.....	13
3.2.2 Fitted Energy-Volume Diagrams .....	15
3.3 In Situ Variable Pressure Powder X-ray Diffraction Experiments .....	18
3.3.1 Birch-Murnaghan Fits.....	18
3.3.2 Bulk Moduli Values.....	19
3.3.3 Powder X-ray Diffraction Patterns .....	19
3.3.4 Selected Fits .....	21
3.3.5 Refinement Results.....	26
4. Additional References .....	38

## Other Supplementary Materials Accompanying this Manuscript:

NU-2003.cif (CCDC: 2347333)

## 1. Experimental Methods

### 1.1 Material Synthesis and Preparation

\*\*\*Safety Caution: Parr vessels used in this study are equipped with a rupture disc built into the vessel head. At extreme pressures this double disc will blow out and release the pressure through an opening in the cover. Do not use pressure vessels without a safety rupture disc.\*\*\*

#### 1.1.1 Single Crystals of NU-2003

Single crystals of NU-2003, reported here for the first time, were synthesized by adding 155 mg (0.99 mmol) of vanadium trichloride and 38 mg (0.24 mmol) of bicyclo[1.1.1]pentane-1,3-dicarboxylic acid (BPDCA) to 2 mL of water in a 23 mL Teflon-lined stainless steel Parr vessel. The mixture was heated to 200 °C for 7 days.

#### 1.1.2 Material Synthesis and Preparation for Compression Experiments

The powder form of NU-2003 was prepared by adding 1200 mg (7.629 mmol) VCl<sub>3</sub> and 600 mg (3.84 mmol) bicyclo[1.1.1]pentane-1,3-dicarboxylic acid (BPDCA) to 15 mL of deionized water in a 125 mL Teflon liner. The mixture was sonicated for 15 minutes, prior to sealing in a stainless-steel Parr vessel and heating in a synthetic convection oven for 1 day at 200 °C. After the vessel cooled to room temperature, the solid NU-2003 particles were isolated by centrifugation and washed three times with 10-15 mL of deionized water and three times with 10-15 mL of dimethylformamide (DMF), with at least 30 minutes in between each wash. The solids were then washed with 10-15 mL of acetone three times, leaving the final wash overnight to allow for complete solvent exchange within the pores of the MOF. NU-2003 was activated for 12-16 hours under dynamic vacuum at 150 °C on a Micromeritics SmartVac Prep System prior to characterization. All other materials (NU-2000, NU-2001, NU-2002, and NU-2005) were prepared and activated (desolvated) according to previously reported procedures.<sup>S1-3</sup>

## 1.2 Material Characterization

### 1.2.1 Powder X-ray Diffraction Under Ambient Conditions

Prior to each pressure campaign (see Section 1.3 for details on the pressure campaigns) and addition of the pressure transmitting medium (Fluorinert FC-70), diffraction data of the combined MOF and CaF<sub>2</sub> mixture were collected to verify that both species were present. The data were collected over 1 minute using monochromatic X-rays ( $\lambda = 0.452 \text{ \AA}$ ) at the 17-BM-B beamline at the Advanced Photon Source at Argonne National Laboratory.

### 1.2.2 Single Crystal X-ray Diffraction Experiment for NU-2003

Intensity data of a green, rod-like single crystal of NU-2003 were collected at 111.15 K. A suitable single crystal with dimensions of  $0.02 \times 0.01 \times 0.01 \text{ mm}^3$  was mounted on a MiTeGen loop with paratone oil on an XtaLAB Synergy diffractometer equipped with a micro-focus sealed X-ray tube PhotonJet (Cu) X-ray and a Hybrid Pixel Array Detector (HyPix) detector. The temperature of the crystal was controlled with an Oxford Cryosystems low-temperature device. Data reduction was performed with the CrysAlisPro software using an empirical absorption correction using spherical harmonics, implemented in SCALE3 ABSPACK scaling algorithm with CrysAlisPro 1.171.42.101a (Rigaku Oxford Diffraction, 2023). The structure was solved with the ShelXT structure solution program using the Intrinsic Phasing solution<sup>S4, 5</sup> method and by using Olex2 as the graphical interface. The model was refined with ShelXL using least squares minimization.<sup>S6</sup>

### 1.3 In Situ Variable Pressure X-ray Diffraction Experiments

#### 1.3.1 Experimental Setup

To understand the behavior of NU-2000, NU-2002, NU-2003, and NU-2005 under mechanical pressure, we performed *in situ* variable pressure X-ray diffraction experiments at room temperature using a membrane-driven diamond anvil cell (DAC), according to our previously published procedures.<sup>S7-9</sup> Prior to the X-ray diffraction experiments, the MOF powders were activated under dynamic vacuum on a Micromeritics Smart Vacuum Prep system. Using a mortar and pestle, the samples were gently mixed with the internal pressure standard CaF<sub>2</sub> (~20% v/v). Stainless-steel gaskets (250 μm thick) were indented to ~100 μm using a membrane-driven diamond anvil cell (DAC) with 300 μm culets and drilled with a laser micro-machining system.<sup>S10</sup> The pre-drilled gasket was placed in the cell and the MOF/CaF<sub>2</sub> mixture was packed into the hole, ensuring no loose powder remained on the gasket. The DAC was sealed carefully to ensure the powder was not compressed and an ambient pattern was collected (see Section 1.2.1).

Prior to each pressure campaign, the DAC was reopened, and Fluorinert FC-70 was added to the mixture as a non-penetrating pressure-transmitting medium, to ensure that the sample experienced equal pressure from all directions.<sup>S8</sup> The DAC was resealed and the compression membrane, driven by a methanol syringe pump system, was installed on the DAC. *In situ* variable pressure PXRD data were collected using monochromatic X-rays ( $\lambda = 0.452 \text{ \AA}$ ) at the 17-BM-B beamline at the Advanced Photon Source, Argonne National Laboratory in combination with a Varex 4343CT area detector. After completion of the pressure campaign, which pressurized the sample to ~1 GPa, the sample was depressurized, and an additional set of diffraction data were collected at ambient conditions to assess the material's ability to recover its crystallinity.

#### 1.3.2 Refinement Details

The PXRD patterns were sequentially refined in GSAS-II using the Le Bail method.<sup>S11</sup> The space group and starting unit cell parameters were taken from structures derived from single crystal X-ray diffraction.<sup>S1-3</sup> To determine the system pressure, the (1,1,1) and the (2,2,0) reflections of CaF<sub>2</sub> were refined and the pressure was calculated from the following equation<sup>S7-9</sup>:

$$P = 84.109 * (V_0/V) - 84.113 \quad \text{Eq. 1}$$

The MOF peaks were fit and sequentially refined between 2θ values of 2 and 15 ( $\lambda = 0.452 \text{ \AA}$ ), excluding the aforementioned CaF<sub>2</sub> reflections between 8-8.5 and 13.3-13.5 and peaks that correspond to the stainless-steel gasket between 12.4 and 13. The Le Bail extractions allowed us to determine unit cell parameters for NU-2000, NU-2002, NU-2003, and NU-2005 at each pressure (Figure S14 and Tables S5, S7, S9, and S11).

#### 1.3.3 Bulk Modulus Calculation

We fit the unit cell data from fitting the MOF peaks and the pressure data from fitting the CaF<sub>2</sub> peaks to the Birch-Murnaghan equation of state to calculate the experimental bulk modulus of each material:

$$P(V) = \frac{K_0}{K'_0} \left[ \left( \frac{V}{V_0} \right)^{-K'_0} - 1 \right] \quad \text{Eq. 2}$$

where  $P$  is the pressure of the system calculated from Eq. 1,  $V$  is the unit cell volume fit from the MOF peaks,  $V_0$  is the initial unit cell volume of the MOF,  $K_0$  is the bulk modulus, and  $K'_0$  is the first derivative of the bulk modulus.<sup>S12</sup> We fit the parameters  $K_0$  and  $K'_0$  using EOSFit7-GUI.<sup>S13, 14</sup>

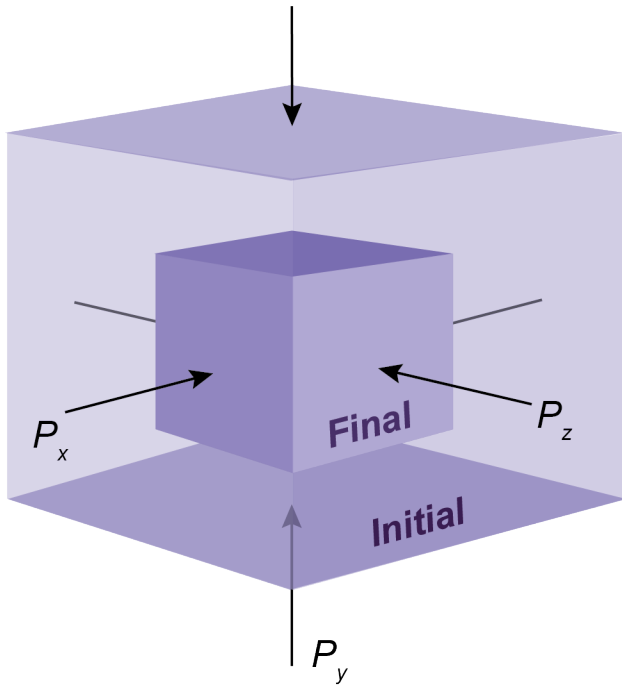


Figure S1. Schematic representation of bulk modulus, i.e. a material's resistance to compression when subjected to uniform pressure ( $P_x=P_y=P_z$ ).

## 2. Computational Methods

### 2.1 Density Functional Theory (DFT) Geometry Optimizations

The 3DL-based structures were built by replacing the 1,4-benzene-dicarboxylate (BDC) linker component in the closed pore and open pore single crystal structures of MIL-53(Al) with the corresponding 3DL linker component using an open source Julia package called PoreMatMod, which employs a “find-and-replace” algorithm that allows for modification of MOF crystal structures.<sup>S15</sup> In the case of the MIL-47(V) structure and its 3DL analogues, the Al nodes were changed to V nodes and the  $\mu$ -OH groups were converted to  $\mu$ -O groups in Materials Studio (v5.0.0.0). Because we previously found that NU-2001 has extra BODCA linkers stuck in 50% of the unit cells after washing and activation (Figure S2), we used the published single crystal structure (CCDC No. 2151358),<sup>S1</sup> rather than building the structure as described above. The atoms and unit cells of these structures were optimized with periodic density functional theory (DFT), performed with VASP (v.5.4.4)<sup>S16-18</sup> at the PBE-D3(BJ) level of theory.<sup>S19-21</sup> We used a projector-augmented plane-wave (PAW) basis set,<sup>S16, 17, 22</sup> with an energy cutoff of 520 eV and a 1x1x1 k-point grid. The self-consistent energy convergence criterion was set to  $10^{-6}$  eV. The spins on vanadium atoms in the vanadium-oxo chains were considered to be in antiferromagnetic arrangement, as previous investigations of MIL-47(V) demonstrate that antiferromagnetic spin results in lower electronic energy than the ferromagnetic spin state in this system.<sup>S23</sup> We also used a Hubbard U correction of 3.1 eV to correct for electron over-delocalization of the vanadium atoms.<sup>S24</sup>

To generate the energy-volume diagrams, we interpolated and extrapolated atomic positions between the narrow pore and large pore structures to generate input files of different volumes. Using the

same parameters as described above, we performed fixed volume geometry optimizations ( $0.01\text{ eV}/\text{\AA}$  convergence criterion for forces was considered), allowing only the shape of the unit cell and the positions of the atoms to change. The energies from each geometry optimization were extracted and plotted against volume.

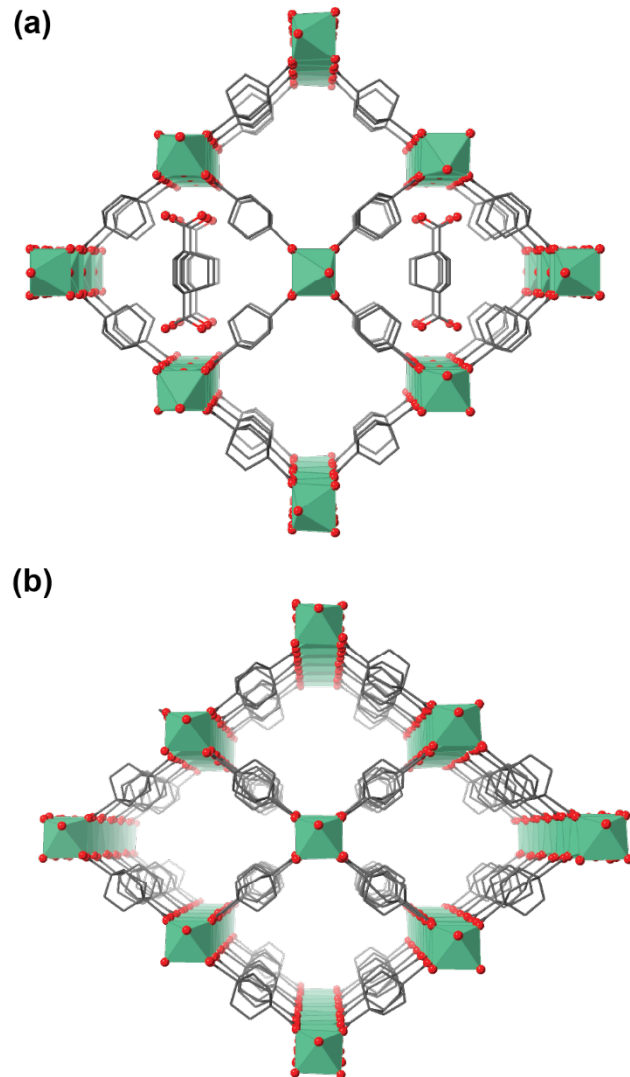


Figure S2. (a) Crystal structure of NU-2001 (CCDC No. 2151358) showing additional linkers that remain in 50% of the unit cells after washing and activating. (b) Hypothetical structure of NU-2001 (no guest) without additional linkers in the pores.

## 2.2 Young's Moduli Calculations

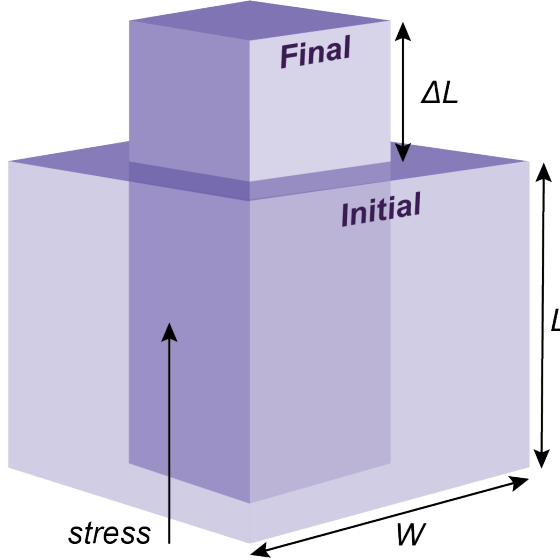


Figure S3. Schematic representation of Young's modulus, i.e. a material's resistance to deformation when a unidirectional stress is applied.

The spatial dependence of the Young's modulus was obtained from the elastic tensor. The elastic tensor can be derived from the generalized Hooke's law:

$$\sigma_{ij} = C_{ijkl}\epsilon_{kl}, \quad \text{Eq. 3}$$

where  $\sigma_{ij}$ ,  $C_{ijkl}$  and  $\epsilon_{kl}$  represent stress tensor, elastic tensor and the strain tensor, respectively. While  $\sigma_{ij}$  and  $\epsilon_{kl}$  are 3x3 tensors,  $C_{ijkl}$  is a 3x3x3x3 tensor. For simplification, we use Voigt notation where strain and stress tensors are expressed as 6 elements vectors, and the elastic tensor is simplified to a 6x6 matrix. For details, please refer to the book by Nye.<sup>S25</sup>

At least six linearly independent strains are required to solve the stress-strain equation (above). Initially, we tried to apply universal linear independent coupling strains as proposed by Yu et al.<sup>S26</sup> However, the resulting elastic constant had negative eigenvalues, suggesting structural instability of the crystal. We attribute this to the high flexibility of the studied MOFs represented by a very shallow/flat potential energy surface.

Instead, we followed the workflow used in the Materials Project,<sup>S27</sup> deforming the unit cells according to the collection of normal ( $\epsilon_1, \epsilon_2, \epsilon_3$ ) and shear ( $\epsilon_4, \epsilon_5, \epsilon_6$ ) strains:

$$\epsilon_1 = \begin{bmatrix} \delta \\ 0 \\ 0 \\ 0 \\ 0 \\ 0 \end{bmatrix}, \epsilon_2 = \begin{bmatrix} 0 \\ \delta \\ 0 \\ 0 \\ 0 \\ 0 \end{bmatrix}, \epsilon_3 = \begin{bmatrix} 0 \\ 0 \\ \delta \\ 0 \\ 0 \\ 0 \end{bmatrix}, \epsilon_4 = \begin{bmatrix} 0 \\ 0 \\ 0 \\ 2\delta \\ 0 \\ 0 \end{bmatrix}, \epsilon_5 = \begin{bmatrix} 0 \\ 0 \\ 0 \\ 0 \\ 2\delta \\ 0 \end{bmatrix}, \epsilon_6 = \begin{bmatrix} 0 \\ 0 \\ 0 \\ 0 \\ 0 \\ 2\delta \end{bmatrix}, \quad \text{Eq. 4}$$

with  $\delta \in \{-0.01, -0.005, +0.005, +0.01\}$ . These strains were converted to the deformation gradients ( $F$ ) by solving the equation for the Green-Lagrange strain<sup>S27</sup> (which can be solved by the Cholesky decomposition method, e.g., with `scipy.linalg.cholesky()`):

$$\boldsymbol{\epsilon} = \frac{1}{2}(\mathbf{F}^T \mathbf{F} - \mathbf{I}) \quad \text{Eq. 5}$$

The deformation gradient was applied to the lattice vectors of the MOF unit cell. Next, for each deformed unit cell (24 per MOF structure) fixed volume and shape geometry optimization was performed within VASP software (see above for the details on the DFT calculations) to obtain the stress tensors. Finally, the elastic tensor (6x6 matrix) was obtained from least-squares fit of the independent strain-stress relations, followed by symmetrization ( $\mathcal{C}_{sym.} = (\mathcal{C}_{ijkl}^T + \mathcal{C}_{ijkl})/2$ ) and IEEE conversion (IEEE standard on piezoelectricity. ANSI/IEEE Std 176-1987 0-1 (1988)).

In our calculations we used the pymatgen subpackage pymatgen.analysis.elasticity for generating strained structures and postprocessing the obtained stresses to calculate the elastic tensor. Finally, a function from the Elate package<sup>S28</sup> was used to calculate the spatial dependence of the Young's modulus from the elements of the compliance tensor  $\mathbf{S}_{ijkl}$ , which is the inverse of the elastic tensor.

### 2.3 Grand Canonical Monte Carlo Simulations

We simulated argon adsorption at 87 K and between 0 and 1 bar in the DFT optimized narrow pore and large pore structures of MIL-53 and 3 structures of NU-2002 (with volumes of 1104, 1126, and 1151 Å<sup>3</sup>) using grand canonical Monte Carlo simulations. These calculations were performed using the gRASPA code, an open-source code for Monte Carlo simulation which uses graphical processing units (GPU).<sup>S29</sup> When performing the simulations, we used 250,000 cycles for initialization and production at each pressure point along the argon isotherm. We included translation, rotation, reinsertion, and swap (insertion or deletion) moves as the Monte Carlo moves, with all moves being randomly selected at equal probabilities.

We used Lennard-Jones parameters from the Dreiding force field for the framework atoms (Al, C, H, and O)<sup>S30</sup> and from TraPPE for the argon adsorbate atoms.<sup>S31</sup> Lorentz-Berthelot mixing rules were applied for the Lennard-Jones interactions between different pseudo-atoms. We used a 12.0 Å cutoff distance for Lennard-Jones interactions and tail correction for guest-guest interactions only.

Table S1. Lennard-Jones parameters used in GCMC simulations.

Atom	$\epsilon/k$ (K)	$\sigma$ (Å)
O	48.1581	3.03315
C	47.8562	3.47299
H	7.64893	2.84642
Al	155.998	3.91105
Ar	115.0	3.407

### 3. Supplemental Text and Additional Results

#### 3.1 Material Characterization

##### 3.1.1 Powder X-ray Diffraction under Ambient Conditions

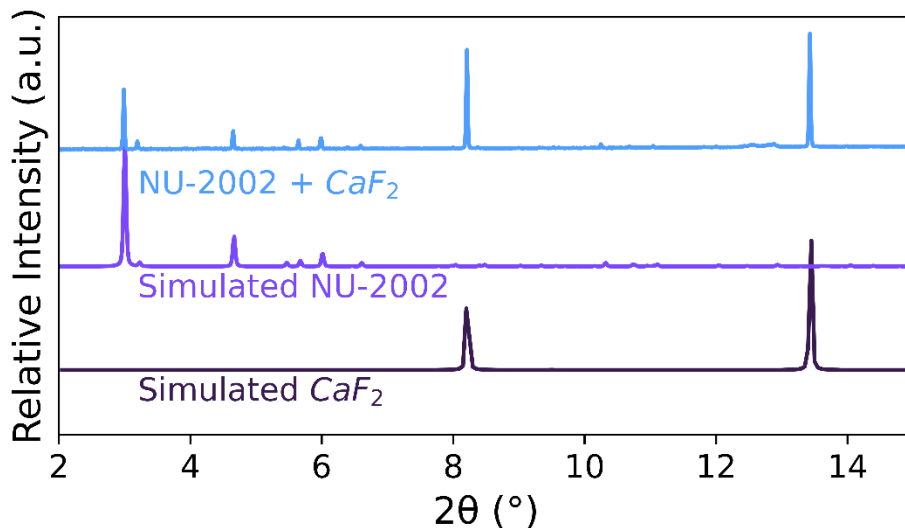


Figure S4. Simulated patterns of CaF<sub>2</sub> (CCDC No. 1603773)<sup>S32</sup> and NU-2002 (CCDC No. 2234124)<sup>S2</sup> compared to mixture collected at ambient conditions, prior to pressurization experiment ( $\lambda = 0.452 \text{ \AA}$ ).

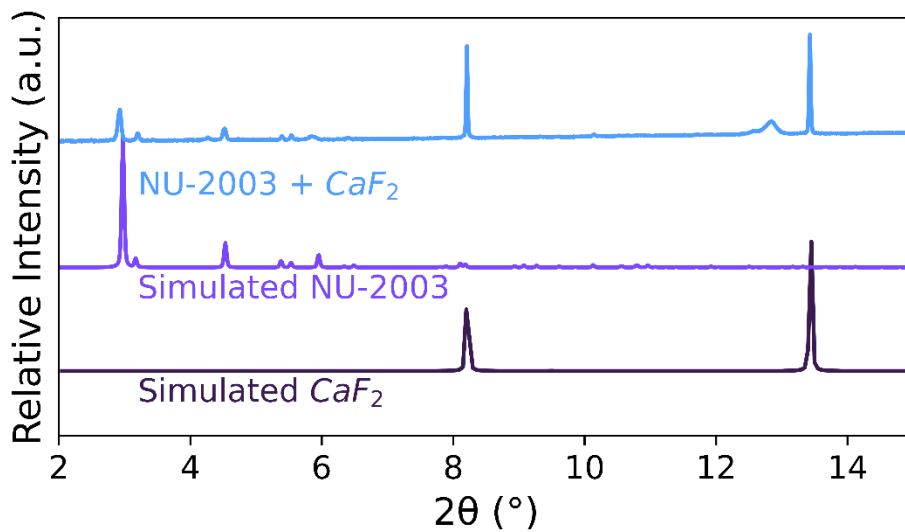


Figure S5. Simulated patterns of CaF<sub>2</sub> (CCDC No. 1603773)<sup>S32</sup> and NU-2003 (CCDC No. 2347333) compared to mixture collected at ambient conditions, prior to pressurization experiment ( $\lambda = 0.452 \text{ \AA}$ ).

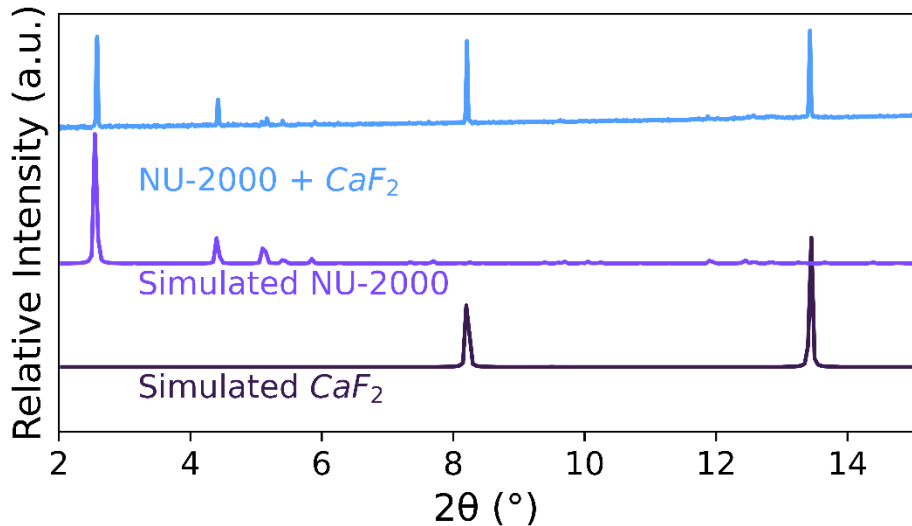


Figure S6. Simulated patterns of CaF<sub>2</sub> (CCDC No. 1603773)<sup>S32</sup> and NU-2000 (CCDC No. 2151356)<sup>S1</sup> compared to mixture collected at ambient conditions, prior to pressurization experiment ( $\lambda = 0.452 \text{ \AA}$ ).

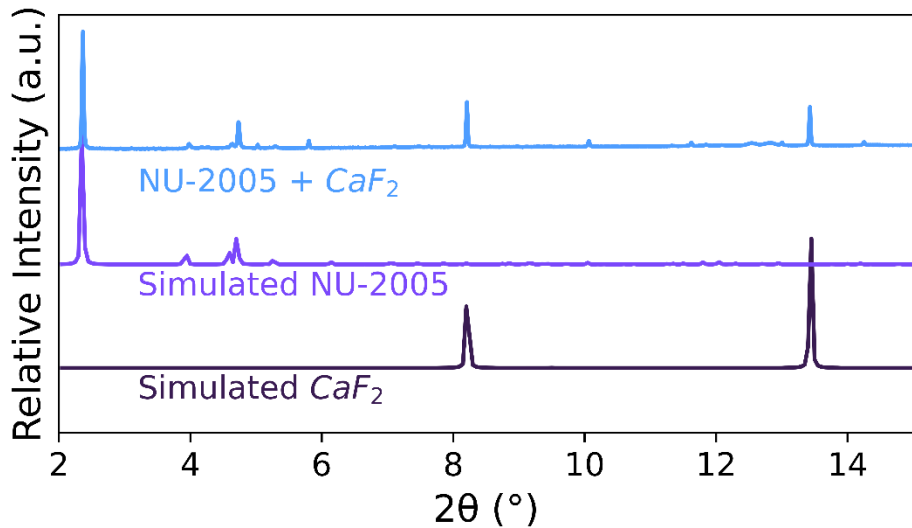


Figure S7. Simulated patterns of CaF<sub>2</sub> (CCDC No. 1603773)<sup>S32</sup> and NU-2005 (CCDC No. 2260499)<sup>S3</sup> compared to mixture collected at ambient conditions, prior to pressurization experiment ( $\lambda = 0.452 \text{ \AA}$ ).

### 3.1.2 Crystallographic Information for NU-2003

Table S2. Crystal data and structural refinement for NU-2003

Empirical formula	C <sub>7</sub> H <sub>2.4</sub> O <sub>6.2</sub> V
Formula weight	236.63
Temperature (K)	111.15
Crystal system	orthorhombic
Space group	Imma
a (Å)	16.342(3)
b (Å)	6.8717(8)
c (Å)	10.284(3)
α=β=γ (°)	90
Volume (Å <sup>3</sup> )	1154.9(4)
Z	4
ρ <sub>calc</sub> (g/cm <sup>3</sup> )	1.361
M (mm <sup>-1</sup> )	7.279
F(000)	468
Crystal size (mm <sup>3</sup> )	0.02 × 0.01 × 0.01
Radiation	CuKα (λ = 1.54184)
2Θ range for data collection (°)	10.162 to 134.882
Index ranges	-19 ≤ h ≤ 19, -7 ≤ k ≤ 8, -12 ≤ l ≤ 12
Reflections collected	5436
Independent reflections	594 [R <sub>int</sub> = 0.1071, R <sub>sigma</sub> = 0.0308]
Data/restraints/parameters	594/10/45
Goodness-of-fit on F <sup>2</sup>	1.594
Final R indexes [I ≥ 2σ (I)]	R <sub>1</sub> = 0.1448, wR <sub>2</sub> = 0.3655
Final R indexes [all data]	R <sub>1</sub> = 0.1523, wR <sub>2</sub> = 0.3719
Largest diff. peak/hole (e Å <sup>-3</sup> )	1.71/-0.53

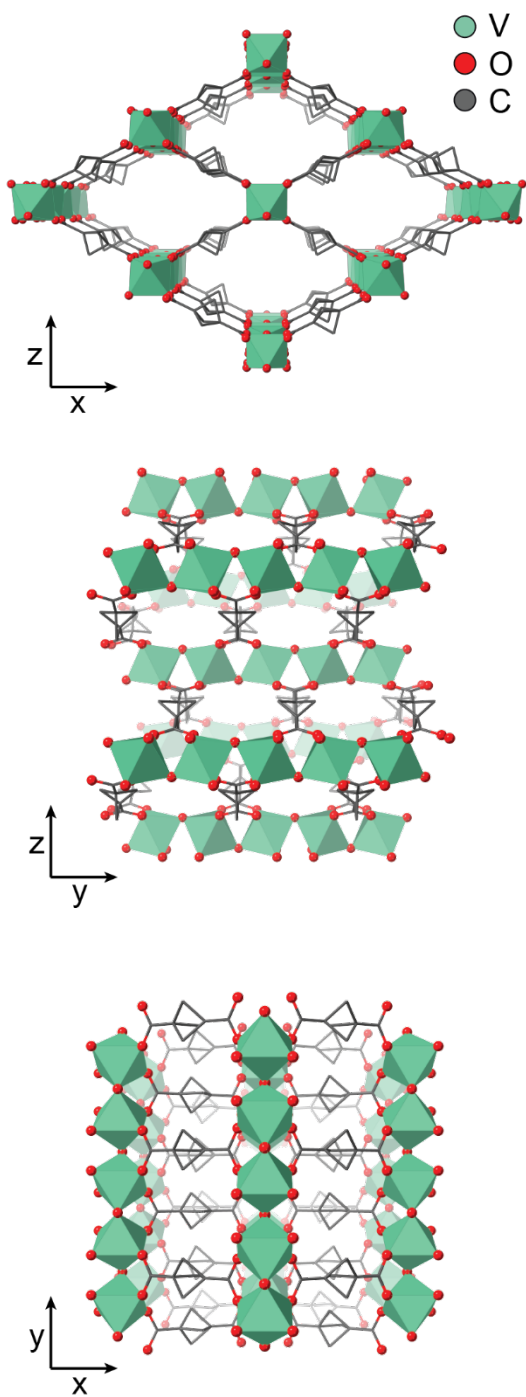


Figure S8. Single crystal X-ray diffraction (SCXRD) structure of NU-2003 (hydrogen atoms omitted for clarity).

### 3.2 Computational Results

#### 3.2.1 Optimized Condensed Phases from DFT Calculations

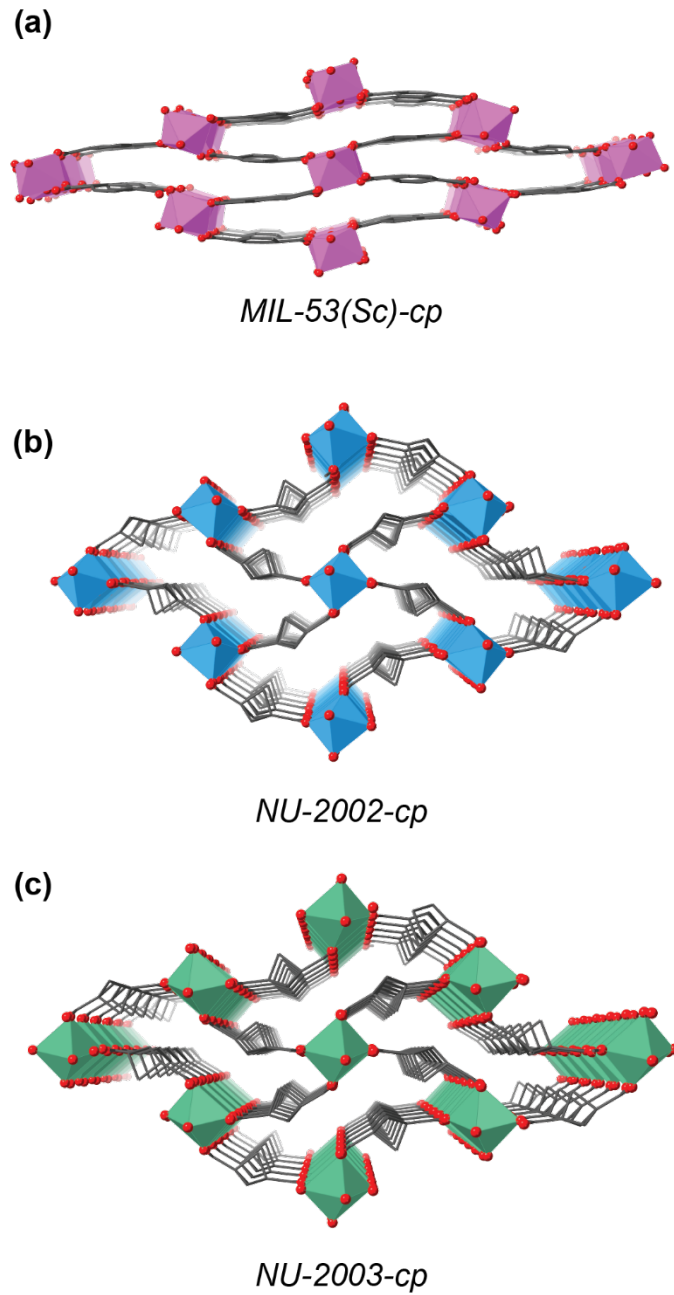


Figure S9. Closed pore phases of (a) MIL-53(Sc) (CCDC No. 844243),<sup>S33</sup> (b) NU-2002, and (c) NU-2003.

The electronic energy profiles of both NU-2002 and NU-2003 demonstrate additional local energy minima at lower volumes, corresponding to condensed phases that are analogous to the condensed phase in MIL-53(Sc) (Figure S9).<sup>S33</sup> The slope of the tangent line between the two minima yields the pressure required to stabilize this phase ( $P(V) = -\frac{\partial E(V)}{\partial V}$ ).<sup>S34</sup> From this analysis, the systems would need to reach approximately 0.22 and 0.15 GPa to stabilize this condensed phase in experimental conditions

for NU-2002 and NU-2003 respectively (Figure S10 and Table S3). However, this only considers the electronic energy contributions, not entropic or thermal effects.<sup>S35</sup> Given that these high-pressure experiments were performed at room temperature, the open pore phase of NU-2002 and NU-2003 is further stabilized, which is why this condensed form is not realized in our experimental results. Therefore, although the structures built from the BPDCA linker exhibit two local minima, the open pore phases are more stable, making switching between the two phases more difficult than in MIL-53.

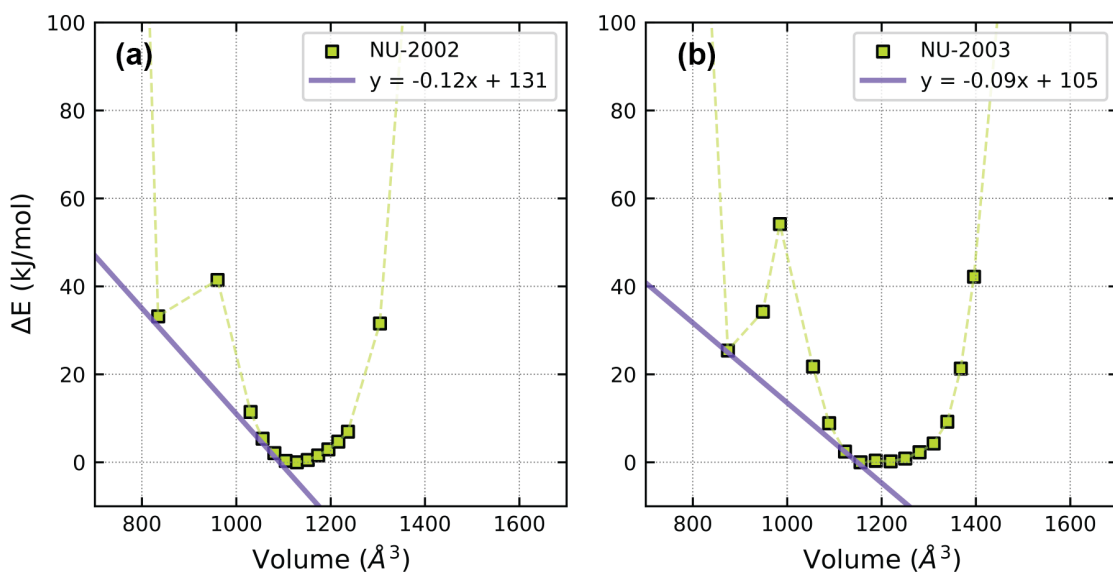


Figure S10. Tangent lines between two local minima in Al and V structures built from BPDCA ligand (NU-2002 and NU-2003, respectively).

Table S3. Electronic energy minima and tangent line values for DFT optimized values of the condensed and ambient phases of NU-2002 and NU-2003 (structures containing the BPDCA linker). The pressure required to reach the condensed phase from the ambient phase is the slope of the tangent line converted to GPa. Energies are reported in kJ/mol, where each a mole refers to a unit cell.

MOF	Condensed Phase Volume (Å³)	Ambient Phase Volume (Å³)	Closed Pore Energy (kJ/mol)	Ambient Phase Energy (kJ/mol)	Pressure (GPa)
NU-2002	834	1128	33.2	0	0.22
NU-2003	874	1155	25.4	0	0.15

### 3.2.2 Fitted Energy-Volume Diagrams

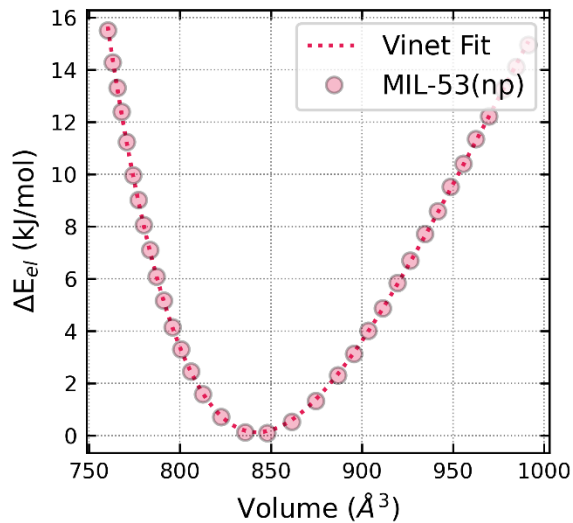


Figure S11. Vinet equation of state fit of energy-volume data of MIL-53(np) generated using DFT by Hoffman *et al.*<sup>S36</sup>

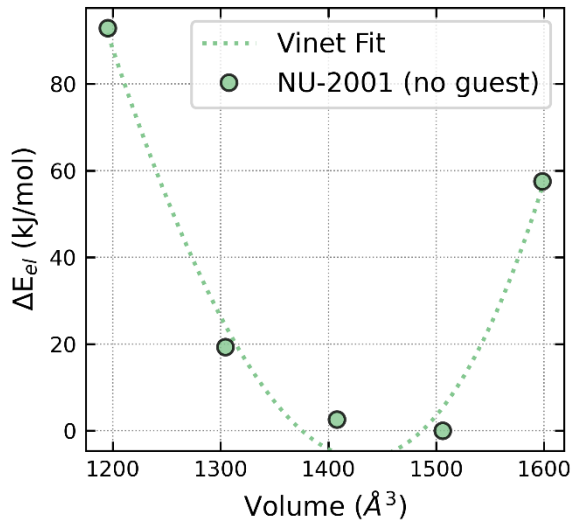


Figure S12. Vinet equation of state fits of energy-volume data generated using DFT for NU-2001 (no guest).

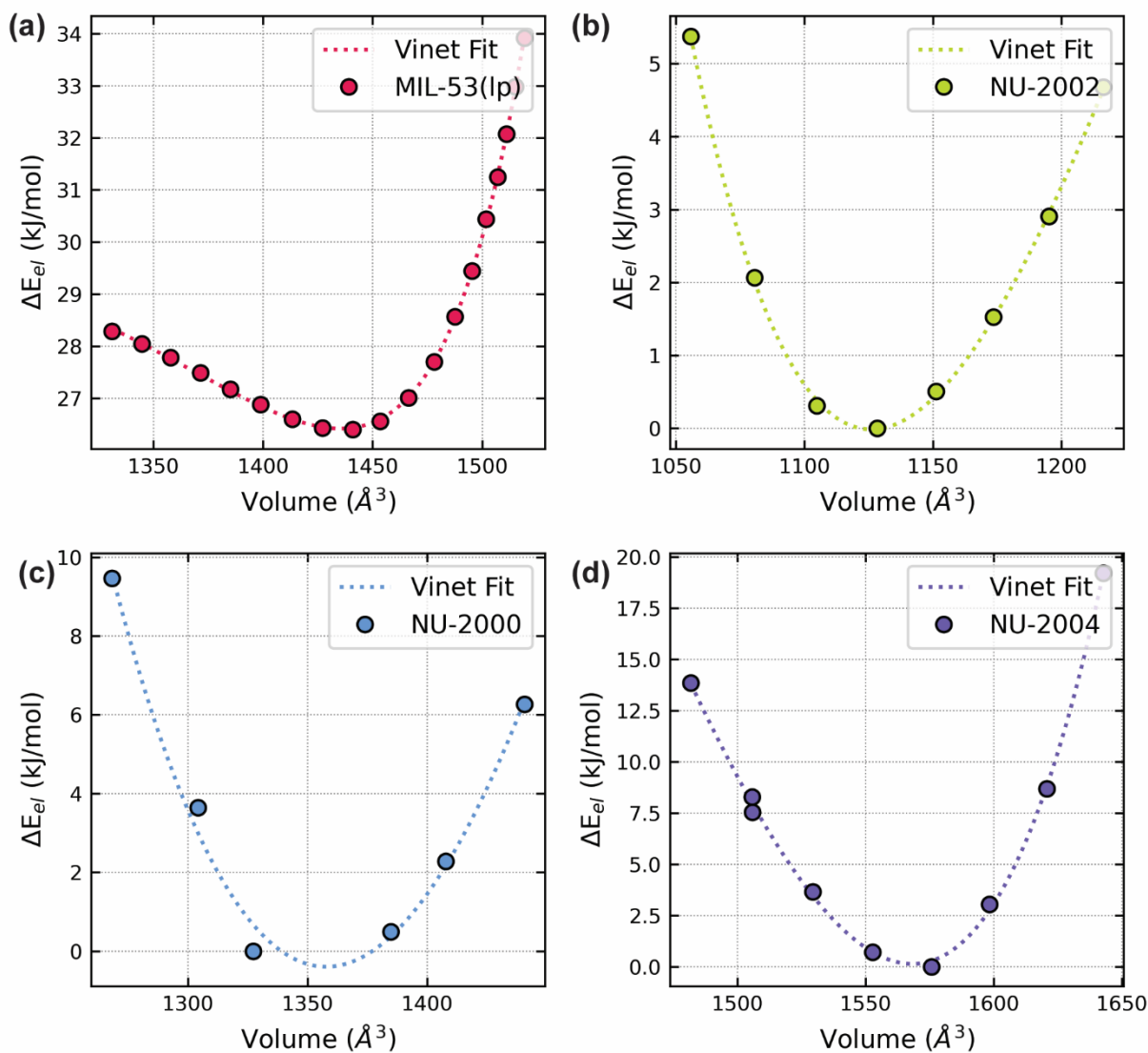


Figure S13. Vinet equation of state fits of energy-volume data generated using DFT for the following aluminum-based structures: (a) MIL-53(lp)<sup>S36</sup>, (b) NU-2002, (c) NU-2000, and (d) NU-2004.

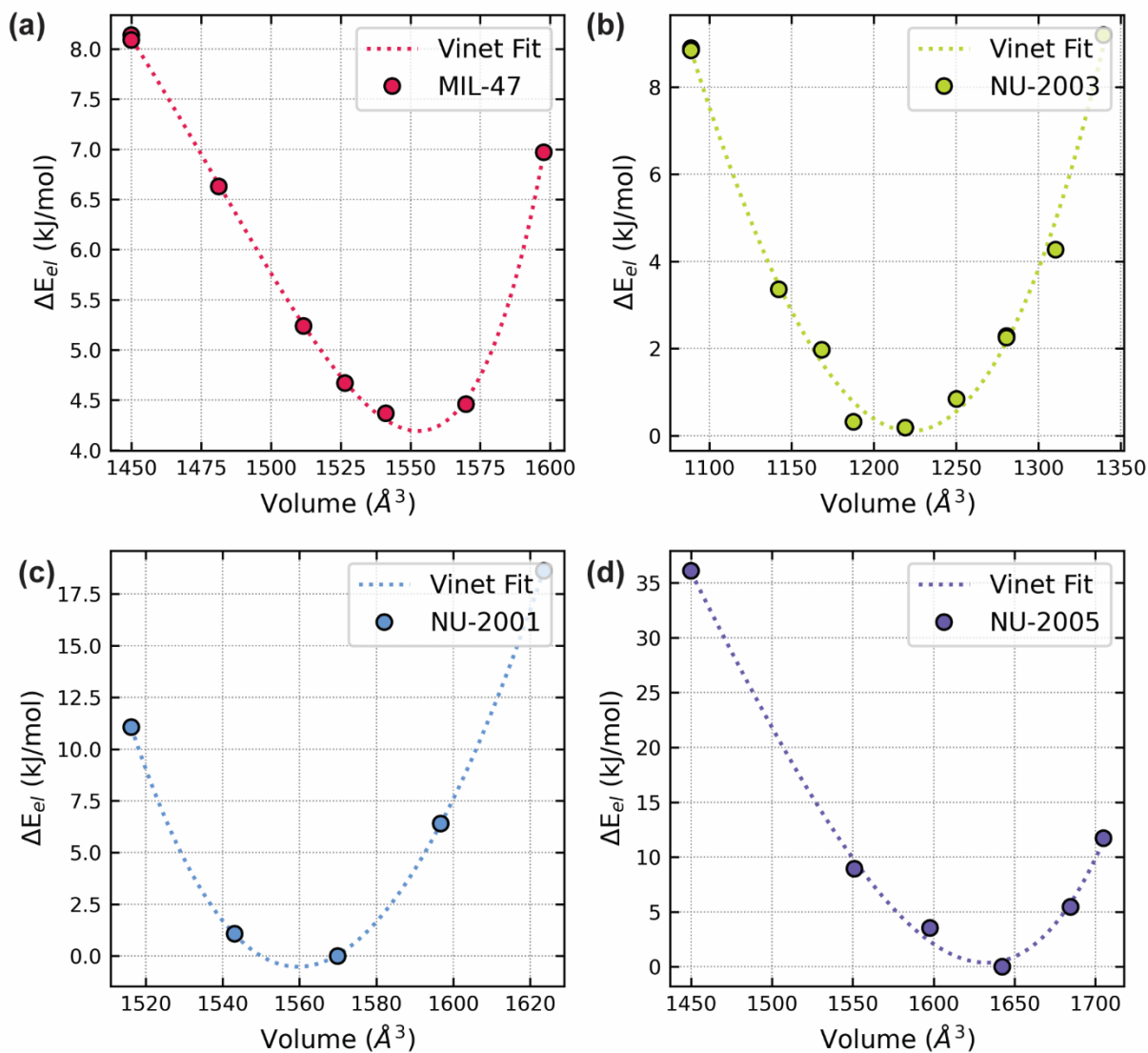


Figure S14. Vinet equation of state fits of energy-volume data generated using DFT for the following vanadium-based structures: (a) MIL-47, (b) NU-2003, (c) NU-2001, and (d) NU-2005.

### 3.3 In Situ Variable Pressure Powder X-ray Diffraction Experiments

#### 3.3.1 Birch-Murnaghan Fits

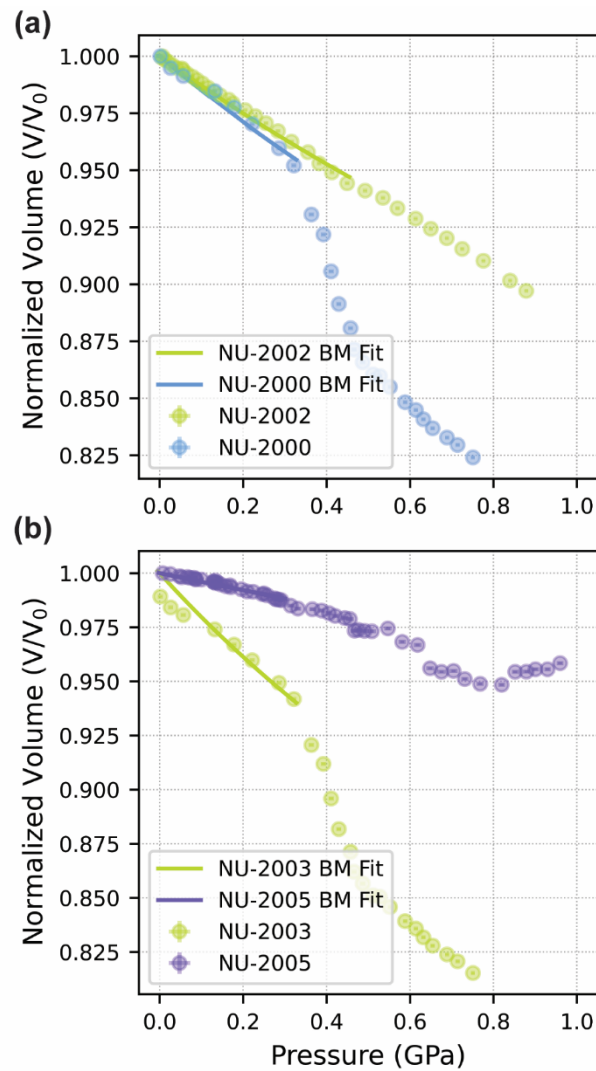


Figure S15. Normalized unit cell volumes fitted from *in situ* powder X-ray diffraction experiments and corresponding Birch-Murnaghan equation of state fits for (a) aluminum structures and (b) vanadium structures.

### 3.3.2 Bulk Moduli Values

Table S4. Values of bulk moduli (K) derived from *in situ* variable pressure X-ray diffraction experiments (PXRD) (Exp. K) and from the fitted energy-volume diagram derived from density functional theory (Comp. K).

	MOF	Exp. K (GPa)	Comp. K (GPa)
Aluminum Nodes	MIL-53(np)	–	1.5 ± 0.01
	MIL-53(lp)	–	1.3 ± 0.01
	NU-2002	7.0 ± 0.1	1.8 ± 0.02
	NU-2000	6.4 ± 0.2	3.0 ± 0.29
	NU-2004	–	8.0 ± 0.15
Vanadium Nodes	MIL-47(V)	–	2.8 ± 0.18
	NU-2003	5.2 ± 0.1	1.4 ± 0.05
	NU-2001 (guest)	–	17.2 ± 0.11
	NU-2001 (no guest)	–	3.5 ± 1.26
	NU-2005	25.0 ± 0.3	5.7 ± 0.79

### 3.3.3 Powder X-ray Diffraction Patterns

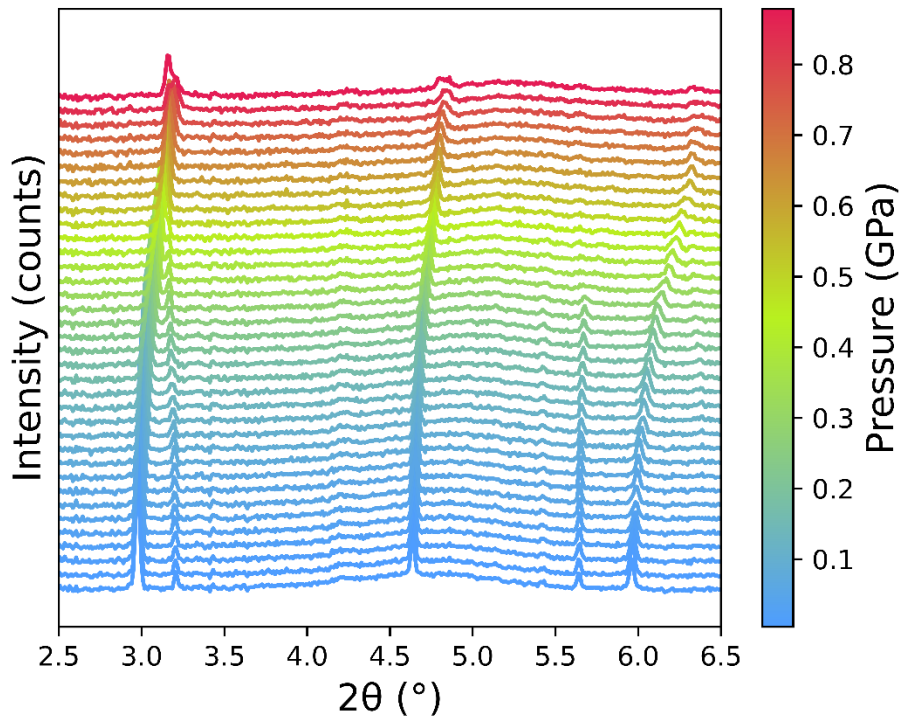


Figure S16. *In situ* variable pressure powder X-ray diffraction patterns for NU-2002.

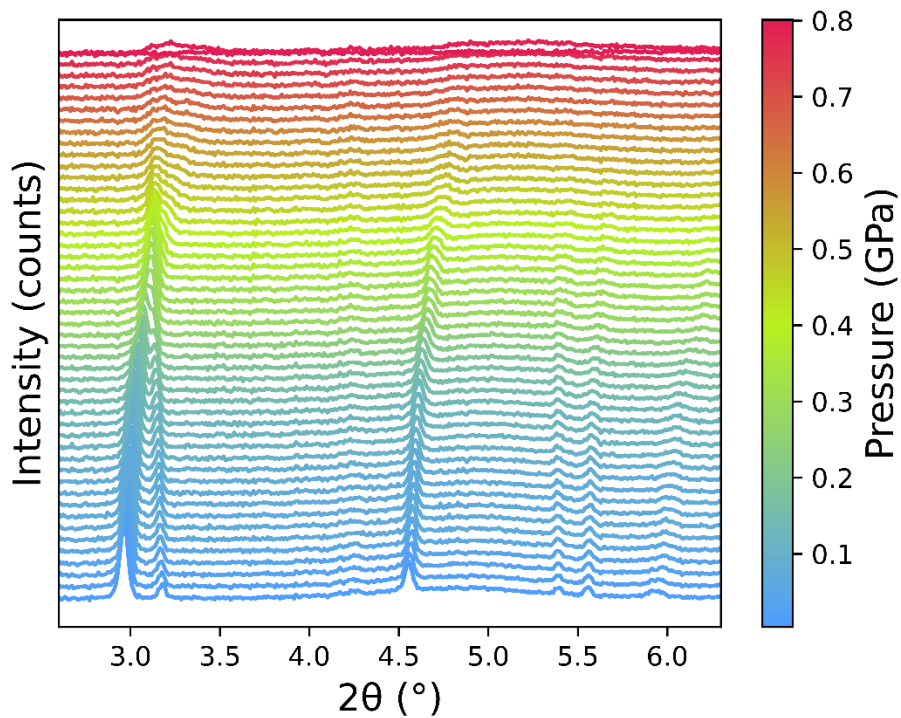


Figure S17. *In situ* variable pressure powder X-ray diffraction patterns for NU-2003.

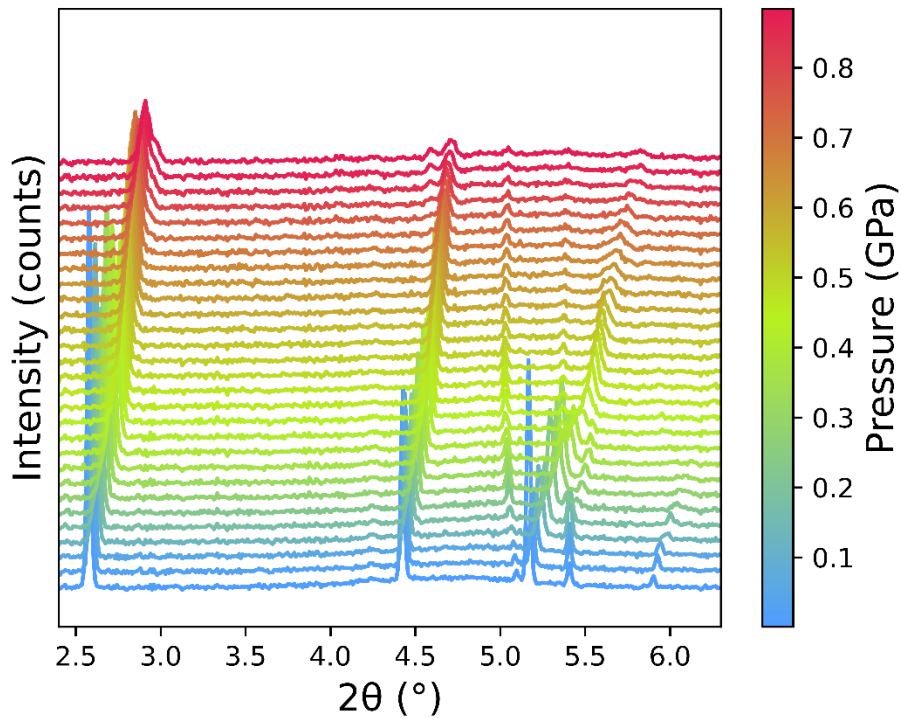


Figure S18. *In situ* variable pressure powder X-ray diffraction patterns for NU-2000.

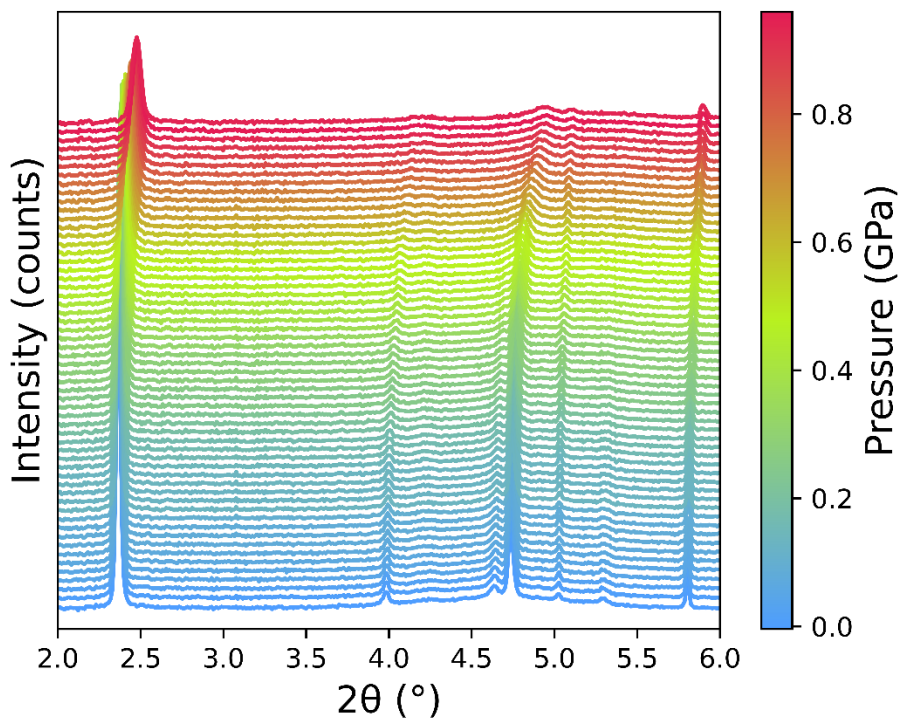


Figure S19. *In situ* variable pressure powder X-ray diffraction patterns for NU-2005.

### 3.3.4 Selected Fits

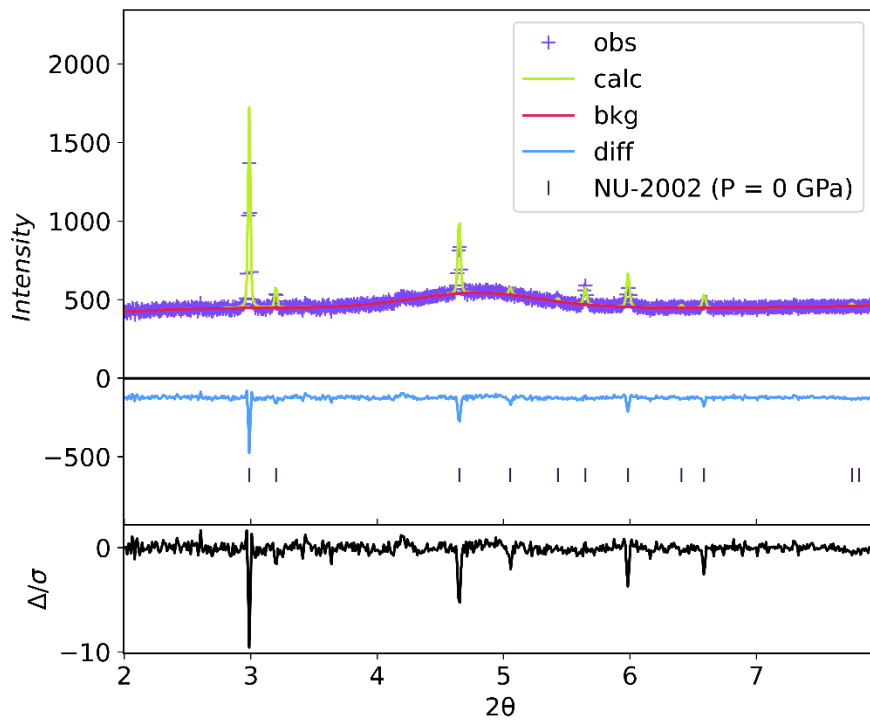


Figure S20. Refinement of NU-2002 at 0 GPa.

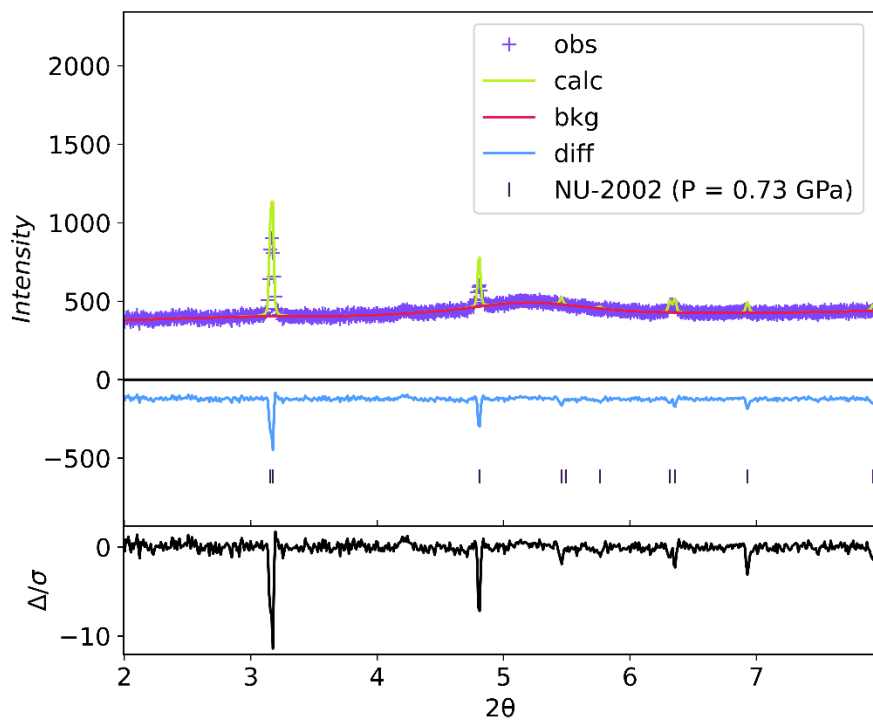


Figure S21. Refinement of NU-2002 at 0.73 GPa.

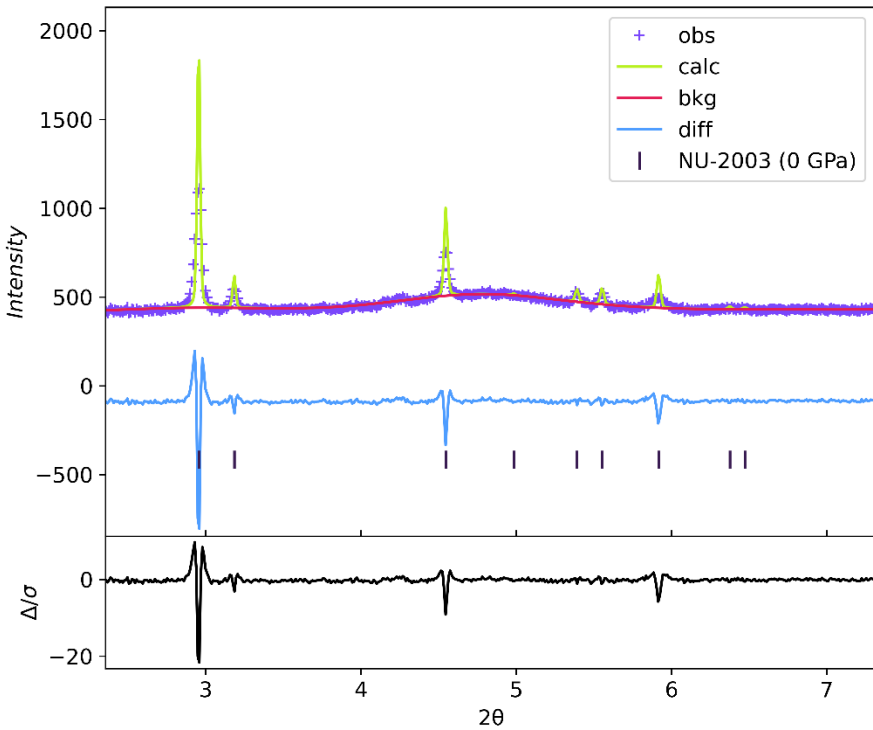


Figure S22. Refinement of NU-2003 at 0 GPa.

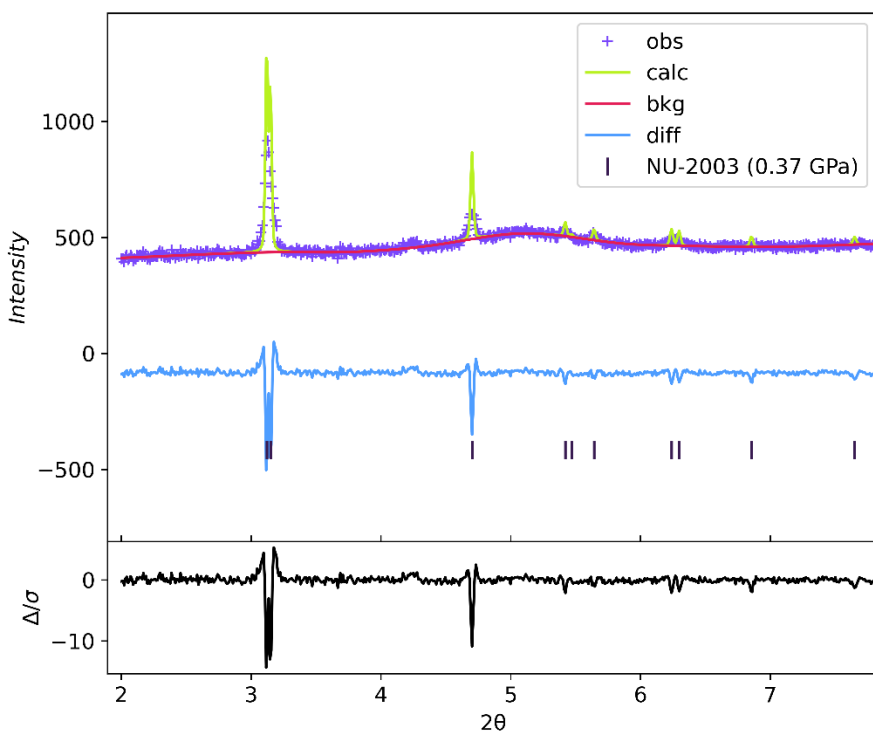


Figure S23. Refinement of NU-2003 at 0.37 GPa.

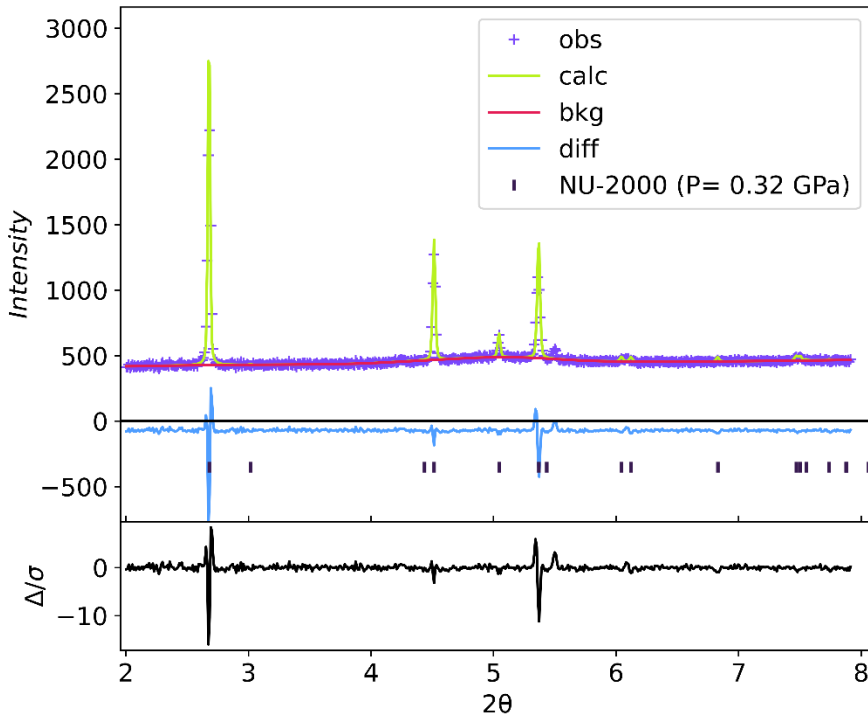


Figure S24. Refinement of NU-2000 at 0.32 GPa.

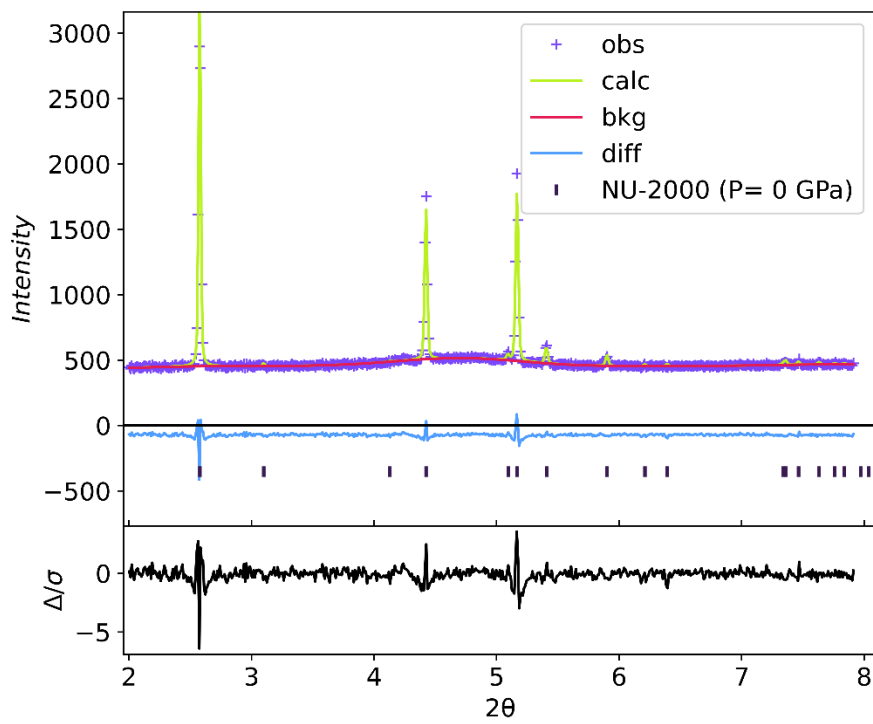


Figure S25. Refinement of NU-2000 at 0 GPa.

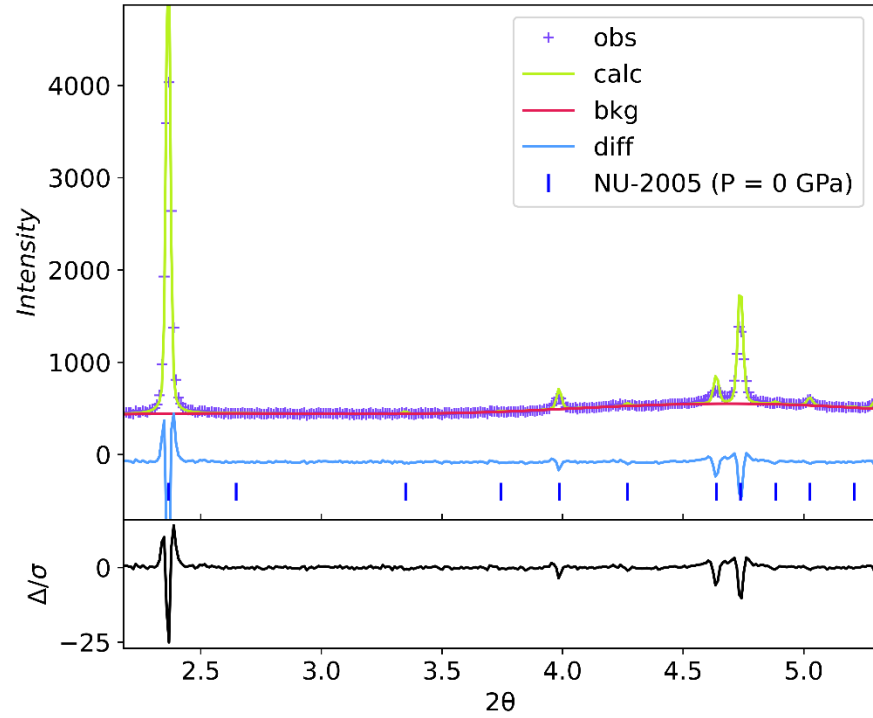


Figure S26. Refinement of NU-2005 at 0 GPa.

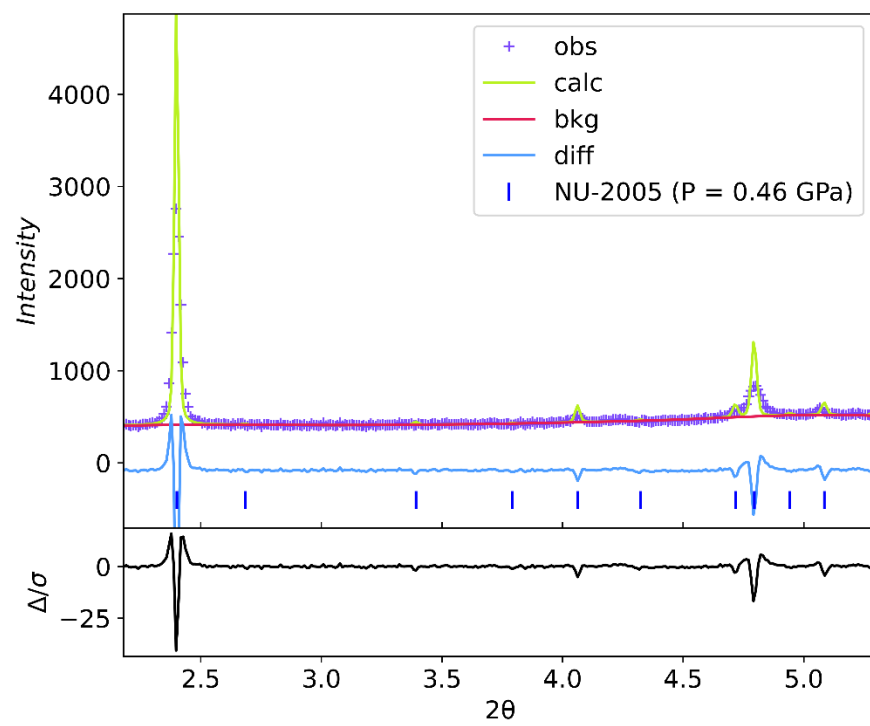


Figure S27. Refinement of NU-2005 at 0.46 GPa.

### 3.3.5 Refinement Results

Table S5. Fitted values of (1,1,1) and (2,2,0) reflections of CaF<sub>2</sub> in the variable pressure X-ray diffraction experiment of NU-2002.

Pattern No.	R <sub>wp</sub>	GOF	a (Å)	a ESD (Å)	Volume (Å <sup>3</sup> )	Volume ESD (Å <sup>3</sup> )	Pressure (GPa)	Pressure ESD (GPa)
1	5.572	1.919	5.455	8.23E-05	162.354	7.35E-03	0.006	5.18E-03
2	5.477	1.882	5.455	8.04E-05	162.358	7.18E-03	0.004	5.12E-03
3	5.325	1.823	5.455	7.80E-05	162.343	6.97E-03	0.012	5.04E-03
4	5.476	1.879	5.455	7.94E-05	162.328	7.09E-03	0.020	5.09E-03
5	5.605	1.930	5.455	7.90E-05	162.309	7.05E-03	0.030	5.07E-03
6	5.657	1.939	5.455	8.06E-05	162.290	7.20E-03	0.040	5.13E-03
7	5.790	1.988	5.454	8.04E-05	162.264	7.18E-03	0.053	5.12E-03
8	5.785	1.977	5.454	8.11E-05	162.260	7.23E-03	0.055	5.14E-03
9	6.124	2.092	5.454	8.39E-05	162.242	7.48E-03	0.065	5.24E-03
10	5.909	2.013	5.454	8.09E-05	162.216	7.22E-03	0.078	5.14E-03
11	5.871	1.993	5.454	8.15E-05	162.194	7.27E-03	0.089	5.16E-03
12	6.143	2.086	5.453	8.37E-05	162.170	7.47E-03	0.102	5.24E-03
13	5.861	1.983	5.453	8.06E-05	162.143	7.19E-03	0.116	5.13E-03
14	5.953	2.014	5.453	8.06E-05	162.119	7.19E-03	0.128	5.13E-03
15	6.279	2.124	5.452	8.31E-05	162.088	7.41E-03	0.144	5.22E-03
16	6.601	2.230	5.452	8.54E-05	162.048	7.61E-03	0.165	5.30E-03
17	6.512	2.199	5.452	8.39E-05	162.029	7.48E-03	0.175	5.25E-03
18	6.125	2.058	5.451	8.25E-05	161.971	7.36E-03	0.205	5.20E-03
19	6.261	2.103	5.451	8.42E-05	161.925	7.51E-03	0.229	5.26E-03
20	6.280	2.106	5.450	8.49E-05	161.876	7.57E-03	0.255	5.29E-03
21	6.268	2.100	5.449	8.56E-05	161.821	7.62E-03	0.283	5.32E-03
22	6.352	2.132	5.449	8.49E-05	161.759	7.56E-03	0.316	5.29E-03
23	6.279	2.107	5.448	8.18E-05	161.683	7.28E-03	0.355	5.19E-03
24	6.355	2.127	5.447	8.42E-05	161.632	7.50E-03	0.382	5.28E-03
25	6.304	2.117	5.447	8.15E-05	161.574	7.25E-03	0.413	5.18E-03
26	6.160	2.062	5.446	8.14E-05	161.504	7.24E-03	0.449	5.19E-03
27	6.197	2.074	5.445	8.19E-05	161.422	7.29E-03	0.492	5.20E-03
28	5.963	1.995	5.444	7.85E-05	161.340	6.98E-03	0.535	5.09E-03
29	5.697	1.907	5.443	7.38E-05	161.273	6.56E-03	0.570	4.94E-03
30	4.962	1.658	5.442	6.54E-05	161.191	5.81E-03	0.613	4.68E-03
31	4.495	1.502	5.441	5.98E-05	161.122	5.31E-03	0.650	4.51E-03
32	4.223	1.410	5.441	5.64E-05	161.049	5.01E-03	0.688	4.42E-03
33	3.965	1.327	5.440	5.28E-05	160.979	4.69E-03	0.725	4.32E-03
34	3.578	1.197	5.439	4.74E-05	160.883	4.20E-03	0.776	4.18E-03
35	3.101	1.037	5.437	4.12E-05	160.762	3.65E-03	0.840	4.04E-03
36	3.106	1.037	5.437	4.13E-05	160.688	3.66E-03	0.879	4.05E-03
37	6.254	2.047	5.455	7.83E-05	162.292	6.99E-03	0.039	5.05E-03

Table S6. Fitted values of NU-2002 peaks from  $2\theta$  values between 2.5 and 15.

Pattern No.	$R_{wp}$	GOF	a (Å)	a ESD (Å)	b (Å)	b ESD (Å)	c (Å)	c ESD (Å)	Volume (Å <sup>3</sup> )	Volume ESD (Å <sup>3</sup> )
1	1.807	0.459	16.133	4.34E-03	6.635	9.32E-04	10.326	1.32E-03	1105.252	2.62E-01
2	1.634	0.414	16.131	3.42E-03	6.637	8.00E-04	10.317	1.08E-03	1104.591	2.13E-01
3	1.649	0.416	16.143	3.57E-03	6.637	6.82E-04	10.301	1.12E-03	1103.626	2.10E-01
4	1.666	0.421	16.146	3.74E-03	6.636	8.44E-04	10.291	1.16E-03	1102.574	2.30E-01
5	1.640	0.416	16.158	3.66E-03	6.634	7.92E-04	10.270	1.09E-03	1100.955	2.21E-01
6	1.652	0.417	16.165	3.13E-03	6.634	7.30E-04	10.254	9.54E-04	1099.629	1.95E-01
7	1.660	0.419	16.167	3.16E-03	6.633	7.54E-04	10.252	1.01E-03	1099.332	1.98E-01
8	1.575	0.396	16.167	3.29E-03	6.633	6.83E-04	10.244	1.03E-03	1098.556	1.97E-01
9	1.704	0.427	16.176	3.72E-03	6.632	8.86E-04	10.224	1.12E-03	1096.893	2.31E-01
10	1.765	0.442	16.178	3.88E-03	6.629	8.11E-04	10.214	1.15E-03	1095.406	2.32E-01
11	1.670	0.417	16.186	3.66E-03	6.631	6.95E-04	10.192	1.10E-03	1093.830	2.14E-01
12	1.730	0.431	16.207	3.36E-03	6.632	7.51E-04	10.161	1.04E-03	1092.135	2.07E-01
13	1.755	0.436	16.213	3.62E-03	6.631	7.69E-04	10.139	1.09E-03	1090.047	2.20E-01
14	1.917	0.476	16.222	4.23E-03	6.629	8.93E-04	10.120	1.26E-03	1088.242	2.57E-01
15	1.985	0.492	16.231	4.37E-03	6.628	9.80E-04	10.099	1.30E-03	1086.383	2.70E-01
16	1.926	0.476	16.246	4.50E-03	6.627	9.89E-04	10.071	1.28E-03	1084.201	2.73E-01
17	1.984	0.490	16.256	4.23E-03	6.625	1.02E-03	10.052	1.23E-03	1082.457	2.68E-01
18	3.058	0.754	16.272	4.16E-03	6.625	1.04E-03	10.009	1.23E-03	1079.047	2.69E-01
19	2.859	0.704	16.283	3.96E-03	6.622	9.48E-04	9.980	1.19E-03	1076.185	2.51E-01
20	2.844	0.699	16.300	4.45E-03	6.623	9.35E-04	9.938	1.26E-03	1072.806	2.71E-01
21	2.912	0.714	16.318	4.07E-03	6.621	1.03E-03	9.895	1.18E-03	1068.990	2.61E-01
22	2.874	0.705	16.332	4.50E-03	6.616	1.02E-03	9.845	1.25E-03	1063.875	2.81E-01
23	2.918	0.715	16.349	5.66E-03	6.614	1.01E-03	9.791	1.43E-03	1058.769	3.32E-01
24	3.068	0.750	16.351	5.55E-03	6.610	1.15E-03	9.746	1.41E-03	1053.325	3.36E-01
25	3.142	0.769	16.364	5.33E-03	6.604	1.16E-03	9.706	1.38E-03	1048.997	3.26E-01
26	3.119	0.762	16.374	4.75E-03	6.598	1.12E-03	9.660	1.27E-03	1043.712	2.99E-01
27	3.137	0.765	16.417	3.88E-03	6.595	1.09E-03	9.607	1.07E-03	1040.090	2.70E-01
28	2.729	0.665	16.436	2.34E-03	6.586	9.87E-04	9.577	1.04E-03	1036.604	2.08E-01
29	2.749	0.669	16.414	1.69E-03	6.577	1.02E-03	9.555	1.17E-03	1031.570	1.92E-01
30	2.841	0.691	16.392	1.43E-03	6.567	1.12E-03	9.537	1.57E-03	1026.566	1.99E-01
31	2.788	0.678	16.370	1.25E-03	6.555	1.19E-03	9.521	1.78E-03	1021.684	2.02E-01
32	3.055	0.743	16.344	1.38E-03	6.547	1.28E-03	9.505	1.89E-03	1017.051	2.22E-01
33	2.987	0.727	16.303	1.57E-03	6.541	1.21E-03	9.489	1.53E-03	1011.902	2.16E-01
34	3.018	0.734	16.257	1.69E-03	6.531	1.28E-03	9.477	1.52E-03	1006.129	2.26E-01
35	3.215	0.781	16.188	1.91E-03	6.504	1.45E-03	9.464	1.65E-03	996.544	2.52E-01
36	3.381	0.819	16.143	1.90E-03	6.488	1.54E-03	9.467	1.85E-03	991.565	2.60E-01
37	1.686	0.408	16.122	2.62E-03	6.629	5.53E-04	10.327	8.62E-04	1103.677	1.58E-01

Table S7. Fitted values of (1,1,1) and (2,2,0) reflections of CaF<sub>2</sub> in the variable pressure X-ray diffraction experiment of NU-2003.

Pattern No.	R <sub>wp</sub>	GOF	a (Å)	a ESD (Å)	Volume (Å <sup>3</sup> )	Volume ESD (Å <sup>3</sup> )	Pressure (GPa)	Pressure ESD (GPa)
1	3.242	1.244	5.465	7.77E-05	163.229	6.96E-03	0.004	5.00E-03
2	3.360	1.293	5.465	8.29E-05	163.198	7.42E-03	0.020	5.18E-03
3	3.642	1.411	5.465	8.97E-05	163.180	8.04E-03	0.029	5.41E-03
4	3.498	1.360	5.464	8.51E-05	163.160	7.62E-03	0.040	5.25E-03
5	3.343	1.308	5.464	7.76E-05	163.136	6.95E-03	0.052	5.00E-03
6	3.442	1.348	5.464	8.38E-05	163.107	7.50E-03	0.067	5.21E-03
7	3.577	1.407	5.464	8.29E-05	163.096	7.42E-03	0.072	5.18E-03
8	3.272	1.285	5.464	7.88E-05	163.106	7.05E-03	0.068	5.04E-03
9	2.869	1.128	5.464	7.32E-05	163.097	6.55E-03	0.072	4.86E-03
10	2.992	1.177	5.464	7.72E-05	163.095	6.91E-03	0.073	4.99E-03
11	3.092	1.219	5.464	8.04E-05	163.088	7.20E-03	0.077	5.10E-03
12	3.309	1.306	5.463	8.44E-05	163.070	7.55E-03	0.086	5.23E-03
13	3.429	1.354	5.463	8.41E-05	163.042	7.53E-03	0.101	5.22E-03
14	3.656	1.447	5.463	8.79E-05	163.022	7.87E-03	0.111	5.36E-03
15	3.708	1.471	5.463	8.94E-05	163.001	8.01E-03	0.122	5.41E-03
16	3.618	1.435	5.463	8.83E-05	163.002	7.90E-03	0.121	5.37E-03
17	3.664	1.453	5.462	8.76E-05	162.977	7.84E-03	0.134	5.35E-03
18	3.555	1.408	5.462	8.59E-05	162.948	7.69E-03	0.149	5.29E-03
19	3.458	1.364	5.462	8.29E-05	162.930	7.42E-03	0.158	5.19E-03
20	4.035	1.594	5.462	9.40E-05	162.906	8.41E-03	0.171	5.58E-03
21	3.819	1.501	5.461	9.00E-05	162.879	8.05E-03	0.185	5.44E-03
22	3.695	1.449	5.461	8.98E-05	162.817	8.03E-03	0.217	5.43E-03
23	3.607	1.412	5.460	8.44E-05	162.772	7.55E-03	0.240	5.25E-03
24	3.593	1.395	5.460	8.87E-05	162.731	7.93E-03	0.261	5.40E-03
25	3.638	1.415	5.459	8.58E-05	162.691	7.67E-03	0.282	5.30E-03
26	3.968	1.541	5.459	9.11E-05	162.664	8.15E-03	0.296	5.49E-03
27	3.590	1.389	5.459	8.57E-05	162.649	7.66E-03	0.304	5.30E-03
28	3.588	1.388	5.459	8.57E-05	162.644	7.66E-03	0.307	5.29E-03
29	3.402	1.313	5.458	8.35E-05	162.578	7.46E-03	0.341	5.22E-03
30	3.401	1.311	5.457	8.42E-05	162.538	7.52E-03	0.362	5.25E-03
31	3.794	1.457	5.457	8.84E-05	162.518	7.90E-03	0.372	5.40E-03
32	3.806	1.463	5.457	8.68E-05	162.484	7.76E-03	0.389	5.34E-03
33	4.016	1.540	5.456	9.43E-05	162.448	8.42E-03	0.408	5.61E-03
34	3.875	1.481	5.456	9.27E-05	162.400	8.28E-03	0.433	5.56E-03
35	3.818	1.462	5.455	8.91E-05	162.360	7.96E-03	0.454	5.43E-03
36	3.796	1.454	5.455	8.81E-05	162.338	7.86E-03	0.465	5.39E-03
37	3.464	1.320	5.455	8.32E-05	162.297	7.43E-03	0.487	5.22E-03
38	3.474	1.320	5.454	8.49E-05	162.245	7.57E-03	0.514	5.28E-03
39	3.313	1.257	5.454	8.11E-05	162.203	7.24E-03	0.536	5.15E-03
40	3.141	1.190	5.453	7.73E-05	162.174	6.90E-03	0.551	5.03E-03

<b>41</b>	3.047	1.156	5.453	7.27E-05	162.134	6.49E-03	0.572	4.88E-03
<b>42</b>	3.069	1.163	5.452	7.16E-05	162.081	6.38E-03	0.600	4.84E-03
<b>43</b>	2.697	1.023	5.451	6.39E-05	162.007	5.70E-03	0.639	4.61E-03
<b>44</b>	2.560	0.970	5.451	6.07E-05	161.954	5.41E-03	0.666	4.51E-03
<b>45</b>	2.214	0.839	5.450	5.34E-05	161.915	4.76E-03	0.687	4.31E-03
<b>46</b>	2.048	0.777	5.450	4.94E-05	161.868	4.40E-03	0.711	4.20E-03
<b>47</b>	2.053	0.778	5.449	4.95E-05	161.806	4.41E-03	0.744	4.21E-03
<b>48</b>	2.090	0.789	5.449	5.00E-05	161.760	4.46E-03	0.768	4.22E-03
<b>49</b>	2.010	0.758	5.448	4.79E-05	161.713	4.26E-03	0.792	4.17E-03
<b>50</b>	1.650	0.504	5.448	1.71E-04	161.697	1.52E-02	0.801	8.73E-03
<b>51</b>	3.984	1.468	5.462	7.94E-05	162.965	7.10E-03	0.140	5.07E-03

Table S8. Fitted values of NU-2003 peaks from  $2\theta$  values between 2.5 and 15.

Pattern No.	$R_{wp}$	GOF	a (Å)	a ESD (Å)	b (Å)	b ESD (Å)	c (Å)	c ESD (Å)	Volume (Å <sup>3</sup> )	Volume ESD (Å <sup>3</sup> )
1	4.509	1.142	16.219	9.00E-03	6.789	1.77E-03	10.305	4.72E-03	1134.773	1.04E+00
2	4.553	1.156	16.258	9.79E-03	6.794	1.88E-03	10.269	5.23E-03	1134.330	1.16E+00
3	5.553	1.418	16.285	9.48E-03	6.796	1.91E-03	10.235	5.21E-03	1132.703	1.18E+00
4	5.338	1.366	16.320	7.37E-03	6.800	1.79E-03	10.223	4.12E-03	1134.552	8.63E-01
5	5.208	1.341	16.340	7.27E-03	6.801	1.77E-03	10.220	4.10E-03	1135.685	8.15E-01
6	5.391	1.390	16.360	7.50E-03	6.805	1.82E-03	10.213	3.87E-03	1137.089	8.64E-01
7	5.344	1.383	16.379	7.14E-03	6.809	1.76E-03	10.200	4.03E-03	1137.437	8.57E-01
8	5.309	1.373	16.394	7.34E-03	6.809	1.82E-03	10.198	4.19E-03	1138.359	9.20E-01
9	5.287	1.370	16.414	7.49E-03	6.812	1.81E-03	10.197	4.10E-03	1140.174	9.38E-01
10	5.459	1.414	16.419	7.39E-03	6.815	1.82E-03	10.171	4.07E-03	1138.139	9.39E-01
11	5.193	1.349	16.438	7.20E-03	6.816	1.74E-03	10.164	3.95E-03	1138.834	8.96E-01
12	5.279	1.372	16.454	7.43E-03	6.816	1.82E-03	10.154	4.30E-03	1138.768	9.37E-01
13	5.275	1.371	16.468	7.29E-03	6.820	1.88E-03	10.124	4.30E-03	1136.963	9.40E-01
14	5.494	1.432	16.429	7.28E-03	6.798	1.93E-03	10.075	4.01E-03	1125.177	9.05E-01
15	5.380	1.405	16.426	6.93E-03	6.793	1.91E-03	10.039	3.91E-03	1120.307	8.80E-01
16	5.476	1.429	16.433	7.11E-03	6.788	1.81E-03	10.022	3.97E-03	1118.017	9.00E-01
17	5.497	1.434	16.452	7.31E-03	6.786	1.88E-03	10.005	4.05E-03	1117.011	9.32E-01
18	5.417	1.411	16.476	7.03E-03	6.785	1.86E-03	9.972	3.86E-03	1114.791	8.97E-01
19	5.387	1.397	16.461	6.56E-03	6.786	1.80E-03	9.910	3.57E-03	1106.982	8.31E-01
20	5.296	1.375	16.494	6.68E-03	6.783	1.79E-03	9.888	3.47E-03	1106.317	8.32E-01
21	5.283	1.365	16.530	6.44E-03	6.783	1.85E-03	9.863	3.43E-03	1105.828	8.37E-01
22	5.368	1.384	16.546	6.33E-03	6.779	1.81E-03	9.812	3.38E-03	1100.510	8.35E-01
23	4.503	1.157	16.590	5.23E-03	6.780	1.57E-03	9.746	2.98E-03	1096.271	7.20E-01
24	4.359	1.113	16.582	4.91E-03	6.767	1.54E-03	9.720	2.83E-03	1090.770	6.74E-01
25	4.134	1.057	16.548	4.23E-03	6.765	1.48E-03	9.684	2.40E-03	1084.185	5.77E-01
26	3.932	1.003	16.537	4.22E-03	6.764	1.48E-03	9.670	2.52E-03	1081.633	5.86E-01
27	3.895	0.990	16.527	4.33E-03	6.764	1.43E-03	9.658	2.57E-03	1079.692	5.98E-01
28	3.958	1.004	16.512	4.34E-03	6.752	1.47E-03	9.645	2.51E-03	1075.427	5.92E-01
29	3.966	1.005	16.513	4.25E-03	6.746	1.55E-03	9.641	2.51E-03	1073.986	5.78E-01
30	4.162	1.053	16.495	4.72E-03	6.736	1.63E-03	9.630	2.69E-03	1070.093	6.35E-01
31	4.198	1.057	16.587	4.87E-03	6.765	1.76E-03	9.459	2.71E-03	1061.344	6.39E-01
32	4.468	1.124	16.561	5.55E-03	6.752	1.90E-03	9.424	3.12E-03	1053.755	7.34E-01
33	--	--	--	--	--	--	--	--	--	--
34	--	--	--	--	--	--	--	--	--	--
35	--	--	--	--	--	--	--	--	--	--
36	--	--	--	--	--	--	--	--	--	--
37	--	--	--	--	--	--	--	--	--	--
38	--	--	--	--	--	--	--	--	--	--
39	--	--	--	--	--	--	--	--	--	--
40	--	--	--	--	--	--	--	--	--	--

<b>41</b>	--	--	--	--	--	--	--	--	--	--	--
<b>42</b>	--	--	--	--	--	--	--	--	--	--	--
<b>43</b>	--	--	--	--	--	--	--	--	--	--	--
<b>44</b>	--	--	--	--	--	--	--	--	--	--	--
<b>45</b>	--	--	--	--	--	--	--	--	--	--	--
<b>46</b>	--	--	--	--	--	--	--	--	--	--	--
<b>47</b>	--	--	--	--	--	--	--	--	--	--	--
<b>48</b>	--	--	--	--	--	--	--	--	--	--	--
<b>49</b>	--	--	--	--	--	--	--	--	--	--	--
<b>50</b>	--	--	--	--	--	--	--	--	--	--	--
<b>51</b>	7.936	1.938	16.077	9.50E-03	6.771	2.19E-03	10.400	5.74E-03	1132.198	1.22E+00	

Table S9. Fitted values of (1,1,1) and (2,2,0) reflections of CaF<sub>2</sub> in the variable pressure X-ray diffraction experiment of NU-2000.

Pattern No.	R <sub>wp</sub>	GOF	a (Å)	a ESD (Å)	Volume (Å <sup>3</sup> )	Volume ESD (Å <sup>3</sup> )	Pressure (GPa)	Pressure ESD (GPa)
1	3.340	1.290	5.465	8.87E-05	163.258	7.95E-03	0.001	5.90E-03
2	3.321	1.301	5.465	8.56E-05	163.209	7.67E-03	0.026	5.81E-03
3	3.419	1.340	5.464	8.56E-05	163.151	7.66E-03	0.056	5.81E-03
4	3.339	1.300	5.463	8.42E-05	163.005	7.54E-03	0.132	5.77E-03
5	3.288	1.276	5.462	8.48E-05	162.916	7.59E-03	0.178	5.79E-03
6	3.257	1.257	5.461	8.65E-05	162.831	7.74E-03	0.222	5.85E-03
7	3.408	1.321	5.459	8.50E-05	162.708	7.60E-03	0.286	5.81E-03
8	3.646	1.410	5.459	9.12E-05	162.639	8.15E-03	0.321	6.01E-03
9	3.941	1.525	5.458	9.27E-05	162.558	8.29E-03	0.363	6.06E-03
10	3.844	1.485	5.457	8.86E-05	162.502	7.92E-03	0.392	5.93E-03
11	3.874	1.495	5.457	9.20E-05	162.467	8.22E-03	0.411	6.04E-03
12	3.524	1.360	5.456	8.41E-05	162.432	7.51E-03	0.429	5.79E-03
13	3.518	1.357	5.456	8.34E-05	162.378	7.45E-03	0.457	5.77E-03
14	3.548	1.369	5.455	8.41E-05	162.361	7.51E-03	0.466	5.79E-03
15	3.577	1.378	5.455	8.59E-05	162.322	7.67E-03	0.486	5.85E-03
16	3.624	1.392	5.454	8.75E-05	162.274	7.81E-03	0.511	5.91E-03
17	3.400	1.304	5.454	8.19E-05	162.242	7.31E-03	0.528	5.73E-03
18	2.673	1.026	5.454	6.55E-05	162.196	5.85E-03	0.552	5.25E-03
19	2.259	0.865	5.453	5.69E-05	162.126	5.08E-03	0.588	5.03E-03
20	2.222	0.853	5.452	5.45E-05	162.077	4.86E-03	0.614	4.98E-03
21	2.343	0.898	5.452	5.50E-05	162.043	4.91E-03	0.632	4.99E-03
22	2.153	0.826	5.451	5.00E-05	162.000	4.46E-03	0.654	4.88E-03
23	1.779	0.680	5.451	4.15E-05	161.935	3.70E-03	0.689	4.70E-03
24	1.636	0.624	5.450	3.88E-05	161.886	3.46E-03	0.714	4.65E-03
25	1.705	0.650	5.449	4.03E-05	161.816	3.59E-03	0.751	4.68E-03
26	1.773	0.674	5.448	4.25E-05	161.733	3.78E-03	0.794	4.73E-03
27	1.673	0.636	5.447	4.03E-05	161.654	3.58E-03	0.836	4.69E-03
28	1.693	0.645	5.447	4.06E-05	161.588	3.61E-03	0.870	4.69E-03
29	1.725	0.654	5.446	4.35E-05	161.561	3.87E-03	0.884	4.75E-03
30	3.628	1.382	5.467	8.32E-05	163.385	7.46E-03	-0.064	5.72E-03

Table S10. Fitted values of NU-2000 peaks from 2θ values between 2.5 and 15.

Pattern No.	R <sub>wp</sub>	GOF	a (Å)	a ESD (Å)	b (Å)	b ESD (Å)	c (Å)	c ESD (Å)	Volume (Å <sup>3</sup> )	Volume ESD (Å <sup>3</sup> )
1	1.902	0.477	6.611	3.81E-04	12.527	1.81E-03	16.677	4.16E-03	1381.089	2.11E-01
2	1.954	0.493	6.608	4.05E-04	12.424	1.71E-03	16.736	3.90E-03	1374.002	2.03E-01
3	2.334	0.589	6.611	5.14E-04	12.338	2.02E-03	16.785	4.64E-03	1369.152	2.47E-01
4	3.102	0.779	6.609	7.48E-04	12.195	2.48E-03	16.873	6.14E-03	1359.890	3.23E-01
5	2.418	0.604	6.602	6.42E-04	12.059	1.76E-03	16.959	4.29E-03	1350.113	2.41E-01
6	2.864	0.712	6.599	6.86E-04	11.933	1.81E-03	17.018	4.62E-03	1339.995	2.72E-01
7	3.721	0.926	6.587	7.61E-04	11.777	1.80E-03	17.086	4.89E-03	1325.390	2.97E-01
8	3.862	0.960	6.579	7.85E-04	11.665	2.04E-03	17.134	6.00E-03	1314.923	3.47E-01
9	4.705	1.167	6.553	9.26E-04	11.617	2.39E-03	16.883	6.69E-03	1285.294	3.87E-01
10	4.364	1.080	6.545	9.27E-04	11.524	3.02E-03	16.880	9.09E-03	1273.096	4.98E-01
11	5.719	1.413	6.528	1.13E-03	11.423	3.79E-03	16.774	1.17E-02	1250.783	6.35E-01
12	5.038	1.245	6.510	9.87E-04	11.362	3.56E-03	16.643	1.12E-02	1231.040	5.98E-01
13	4.588	1.131	6.500	9.86E-04	11.325	3.34E-03	16.524	1.05E-02	1216.378	5.63E-01
14	4.527	1.116	6.489	9.67E-04	11.321	2.55E-03	16.381	7.69E-03	1203.471	4.36E-01
15	4.509	1.110	6.482	9.15E-04	11.290	2.59E-03	16.342	7.51E-03	1195.899	4.15E-01
16	4.665	1.145	6.475	9.20E-04	11.255	2.65E-03	16.307	7.48E-03	1188.347	4.08E-01
17	4.518	1.108	6.480	7.85E-04	11.164	2.33E-03	16.413	6.93E-03	1187.400	3.74E-01
18	4.853	1.192	6.477	8.85E-04	11.123	2.69E-03	16.391	8.39E-03	1180.772	4.49E-01
19	5.153	1.264	6.467	9.73E-04	11.072	2.59E-03	16.363	8.00E-03	1171.637	4.39E-01
20	5.565	1.368	6.465	1.08E-03	11.027	3.17E-03	16.369	1.00E-02	1166.828	5.37E-01
21	5.917	1.453	6.460	1.23E-03	10.989	3.51E-03	16.356	1.11E-02	1161.206	5.92E-01
22	5.964	1.462	6.457	1.26E-03	10.942	3.30E-03	16.360	1.04E-02	1155.831	5.66E-01
23	5.968	1.459	6.452	1.37E-03	10.904	3.49E-03	16.350	1.10E-02	1150.197	5.93E-01
24	6.283	1.532	6.449	1.46E-03	10.862	3.54E-03	16.358	1.13E-02	1145.753	6.13E-01
25	6.145	1.497	6.446	1.52E-03	10.804	3.67E-03	16.343	1.19E-02	1138.163	6.47E-01
26	7.735	1.877	6.442	2.01E-03	10.850	3.64E-03	16.357	1.07E-02	1143.290	6.46E-01
27	--	--	--	--	--	--	--	--	--	--
28	--	--	--	--	--	--	--	--	--	--
29	9.392	2.272	6.444	3.08E-03	10.859	3.12E-03	16.358	6.38E-03	1144.605	6.46E-01
30	5.094	1.263	6.612	7.18E-04	12.507	2.89E-03	16.698	6.52E-03	1380.817	3.40E-01

Table S11. Fitted values of (1,1,1) and (2,2,0) reflections of CaF<sub>2</sub> in the variable pressure X-ray diffraction experiment of NU-2005.

Pattern No.	R <sub>wp</sub>	GOF	a (Å)	a ESD (Å)	Volume (Å <sup>3</sup> )	Volume ESD (Å <sup>3</sup> )	Pressure (GPa)	Pressure ESD (GPa)
1	2.079	0.791	5.466	7.83E-05	163.310	7.02E-03	0.025	4.94E-03
2	1.540	0.589	5.466	6.50E-05	163.268	5.83E-03	0.047	4.51E-03
3	1.589	0.609	5.465	7.14E-05	163.257	6.40E-03	0.052	4.71E-03
4	1.482	0.569	5.465	6.98E-05	163.230	6.25E-03	0.066	4.66E-03
5	1.623	0.624	5.465	7.23E-05	163.219	6.47E-03	0.072	4.74E-03
6	1.525	0.587	5.465	6.43E-05	163.199	5.76E-03	0.082	4.49E-03
7	1.657	0.639	5.465	7.01E-05	163.193	6.28E-03	0.086	4.67E-03
8	1.421	0.547	5.465	6.53E-05	163.192	5.85E-03	0.086	4.52E-03
9	2.073	0.800	5.464	8.91E-05	163.165	7.98E-03	0.100	5.32E-03
10	2.414	0.933	5.464	1.05E-04	163.101	9.44E-03	0.133	5.92E-03
11	2.133	0.824	5.464	9.31E-05	163.111	8.34E-03	0.128	5.47E-03
12	1.829	0.706	5.464	8.08E-05	163.108	7.24E-03	0.130	5.03E-03
13	1.524	0.585	5.464	6.91E-05	163.093	6.18E-03	0.138	4.64E-03
14	1.717	0.657	5.464	8.39E-05	163.100	7.52E-03	0.134	5.14E-03
15	1.716	0.658	5.463	8.02E-05	163.076	7.18E-03	0.146	5.01E-03
16	2.092	0.800	5.463	9.37E-05	163.052	8.39E-03	0.158	5.49E-03
17	2.694	1.028	5.463	1.22E-04	163.033	1.09E-02	0.168	6.57E-03
18	2.680	1.019	5.463	1.13E-04	163.029	1.01E-02	0.170	6.22E-03
19	2.775	1.059	5.462	1.12E-04	162.981	1.00E-02	0.195	6.19E-03
20	2.805	1.068	5.462	1.16E-04	162.954	1.04E-02	0.209	6.36E-03
21	3.073	1.170	5.462	1.32E-04	162.926	1.18E-02	0.224	6.99E-03
22	3.267	1.242	5.461	1.39E-04	162.875	1.24E-02	0.250	7.26E-03
23	3.310	1.261	5.461	1.40E-04	162.883	1.25E-02	0.246	7.31E-03
24	3.029	1.153	5.461	1.24E-04	162.861	1.11E-02	0.257	6.68E-03
25	2.977	1.129	5.461	1.30E-04	162.827	1.16E-02	0.275	6.89E-03
26	3.458	1.311	5.461	1.42E-04	162.818	1.27E-02	0.280	7.40E-03
27	3.848	1.455	5.460	1.69E-04	162.807	1.51E-02	0.285	8.54E-03
28	4.043	1.526	5.460	1.84E-04	162.795	1.65E-02	0.292	9.19E-03
29	3.580	1.350	5.460	1.65E-04	162.752	1.47E-02	0.314	8.36E-03
30	3.533	1.332	5.459	1.50E-04	162.718	1.34E-02	0.331	7.75E-03
31	3.481	1.310	5.459	1.38E-04	162.652	1.23E-02	0.366	7.22E-03
32	3.591	1.351	5.458	1.38E-04	162.610	1.23E-02	0.388	7.24E-03
33	3.823	1.435	5.458	1.38E-04	162.575	1.23E-02	0.406	7.24E-03
34	3.773	1.412	5.457	1.40E-04	162.546	1.25E-02	0.421	7.32E-03
35	3.780	1.408	5.457	1.60E-04	162.503	1.43E-02	0.443	8.17E-03
36	3.968	1.473	5.457	1.82E-04	162.479	1.62E-02	0.456	9.10E-03
37	4.310	1.597	5.456	1.97E-04	162.457	1.76E-02	0.467	9.77E-03
38	4.880	1.806	5.456	2.21E-04	162.440	1.98E-02	0.476	1.08E-02
39	4.956	1.829	5.456	2.35E-04	162.412	2.10E-02	0.491	1.14E-02

<b>40</b>	4.404	1.619	5.456	2.00E-04	162.378	1.78E-02	0.508	9.89E-03
<b>41</b>	3.931	1.445	5.455	1.78E-04	162.304	1.59E-02	0.547	8.95E-03
<b>42</b>	3.976	1.458	5.454	1.79E-04	162.238	1.60E-02	0.581	8.99E-03
<b>43</b>	4.113	1.505	5.453	1.87E-04	162.167	1.67E-02	0.618	9.34E-03
<b>44</b>	4.075	1.487	5.453	1.85E-04	162.110	1.65E-02	0.648	9.25E-03
<b>45</b>	4.258	1.555	5.452	1.98E-04	162.058	1.77E-02	0.675	9.86E-03
<b>46</b>	3.994	1.457	5.451	1.88E-04	162.003	1.67E-02	0.704	9.39E-03
<b>47</b>	3.620	1.320	5.451	1.70E-04	161.951	1.52E-02	0.731	8.64E-03
<b>48</b>	3.520	1.282	5.450	1.68E-04	161.881	1.49E-02	0.768	8.53E-03
<b>49</b>	3.415	1.247	5.449	1.56E-04	161.782	1.39E-02	0.820	8.04E-03
<b>50</b>	3.329	1.218	5.448	1.53E-04	161.721	1.36E-02	0.852	7.91E-03
<b>51</b>	3.299	1.208	5.448	1.53E-04	161.670	1.37E-02	0.879	7.95E-03
<b>52</b>	3.338	1.219	5.447	1.54E-04	161.628	1.37E-02	0.901	7.96E-03
<b>53</b>	3.239	1.183	5.447	1.49E-04	161.574	1.33E-02	0.930	7.78E-03
<b>54</b>	3.366	1.227	5.446	1.58E-04	161.517	1.41E-02	0.960	8.16E-03
<b>55</b>	3.169	1.152	5.446	1.55E-04	161.556	1.38E-02	0.939	8.02E-03
<b>56</b>	3.118	1.136	5.451	1.18E-04	161.988	1.06E-02	0.712	6.48E-03
<b>57</b>	3.188	1.157	5.452	1.32E-04	162.054	1.18E-02	0.677	7.03E-03
<b>58</b>	3.397	1.230	5.452	1.48E-04	162.067	1.32E-02	0.670	7.69E-03
<b>59</b>	2.143	0.799	5.467	7.36E-05	163.360	6.59E-03	-0.001	4.78E-03

Table S12. Fitted values of NU-2005 peaks from 2 $\theta$  values between 2.5 and 15 for the variable pressure X-ray diffraction experiment.

Pattern No.	R <sub>wp</sub>	GOF	a (Å)	a ESD (Å)	c (Å)	c ESD (Å)	Volume (Å <sup>3</sup> )	Volume ESD (Å <sup>3</sup> )
1	4.856	1.218	21.950	1.80E-03	6.828	2.17E-03	3289.398	1.11E+00
2	4.981	1.256	21.946	1.77E-03	6.823	2.14E-03	3286.357	1.09E+00
3	4.959	1.252	21.943	1.96E-03	6.821	2.35E-03	3284.374	1.19E+00
4	4.814	1.217	21.942	1.89E-03	6.823	2.32E-03	3284.862	1.18E+00
5	4.809	1.215	21.942	1.89E-03	6.820	2.32E-03	3283.565	1.18E+00
6	4.719	1.195	21.942	1.91E-03	6.820	2.35E-03	3283.575	1.19E+00
7	4.688	1.188	21.939	1.81E-03	6.819	2.33E-03	3281.956	1.19E+00
8	4.841	1.224	21.938	1.86E-03	6.818	2.34E-03	3281.199	1.18E+00
9	4.775	1.211	21.938	1.96E-03	6.817	2.33E-03	3280.898	1.19E+00
10	4.670	1.186	21.937	1.87E-03	6.814	2.35E-03	3279.186	1.20E+00
11	4.645	1.179	21.934	1.63E-03	6.813	2.40E-03	3277.882	1.20E+00
12	4.783	1.212	21.934	1.22E-03	6.812	2.37E-03	3277.177	1.16E+00
13	4.849	1.223	21.933	1.62E-03	6.811	2.27E-03	3276.713	1.15E+00
14	4.787	1.204	21.931	1.77E-03	6.811	2.42E-03	3275.905	1.21E+00
15	4.895	1.234	21.929	1.75E-03	6.807	2.36E-03	3273.574	1.18E+00
16	4.734	1.190	21.927	1.82E-03	6.803	2.36E-03	3270.984	1.20E+00
17	4.812	1.206	21.926	1.83E-03	6.806	2.34E-03	3272.061	1.20E+00
18	4.799	1.197	21.923	1.85E-03	6.803	2.62E-03	3269.328	1.31E+00
19	6.907	1.730	21.913	1.89E-03	6.802	1.64E-03	3266.238	7.65E-01
20	5.081	1.269	21.916	1.92E-03	6.793	2.52E-03	3262.837	1.27E+00
21	5.198	1.299	21.914	1.96E-03	6.793	2.49E-03	3262.394	1.26E+00
22	5.108	1.274	21.912	1.96E-03	6.789	2.59E-03	3259.720	1.31E+00
23	5.225	1.305	21.910	1.90E-03	6.788	2.74E-03	3258.669	1.37E+00
24	5.347	1.332	21.908	1.91E-03	6.786	2.85E-03	3257.000	1.42E+00
25	5.291	1.313	21.904	1.91E-03	6.779	2.80E-03	3252.412	1.40E+00
26	5.278	1.309	21.899	1.97E-03	6.778	2.97E-03	3250.765	1.47E+00
27	5.363	1.327	21.899	1.94E-03	6.778	3.00E-03	3250.457	1.49E+00
28	5.468	1.351	21.897	2.17E-03	6.777	3.14E-03	3249.524	1.56E+00
29	5.465	1.348	21.890	2.44E-03	6.764	3.06E-03	3241.146	1.56E+00
30	5.637	1.389	21.883	2.65E-03	6.759	3.22E-03	3236.742	1.64E+00
31	5.845	1.438	21.883	2.79E-03	6.757	3.31E-03	3235.750	1.68E+00
32	5.871	1.442	21.880	2.87E-03	6.756	3.55E-03	3234.002	1.79E+00
33	5.910	1.448	21.875	3.00E-03	6.750	3.81E-03	3229.709	1.91E+00
34	6.027	1.473	21.862	3.25E-03	6.749	3.67E-03	3225.547	1.88E+00
35	6.019	1.464	21.852	3.49E-03	6.748	3.86E-03	3222.453	1.96E+00
36	6.105	1.479	21.848	3.45E-03	6.748	4.10E-03	3220.952	2.02E+00
37	6.132	1.483	21.798	3.45E-03	6.741	3.99E-03	3203.127	1.94E+00
38	6.259	1.510	21.796	3.45E-03	6.746	3.95E-03	3204.534	1.92E+00
39	6.316	1.520	21.796	3.54E-03	6.742	4.13E-03	3202.958	1.98E+00

<b>40</b>	6.334	1.517	21.795	3.64E-03	6.742	4.28E-03	3202.342	2.02E+00
<b>41</b>	6.360	1.522	21.782	3.70E-03	6.758	5.00E-03	3206.627	2.32E+00
<b>42</b>	8.896	2.123	21.792	3.46E-03	6.710	3.58E-03	3186.317	1.78E+00
<b>43</b>	9.017	2.146	21.786	3.58E-03	6.703	3.77E-03	3181.469	1.84E+00
<b>44</b>	9.036	2.145	21.661	4.44E-03	6.705	2.79E-03	3146.060	1.36E+00
<b>45</b>	9.065	2.154	21.643	4.57E-03	6.705	3.09E-03	3140.698	1.46E+00
<b>46</b>	9.137	2.169	21.648	4.69E-03	6.705	3.08E-03	3142.055	1.48E+00
<b>47</b>	9.274	2.199	21.580	4.78E-03	6.721	3.19E-03	3129.788	1.45E+00
<b>48</b>	9.462	2.241	21.538	5.12E-03	6.731	2.65E-03	3122.378	1.43E+00
<b>49</b>	9.147	2.169	21.538	5.24E-03	6.728	2.26E-03	3120.919	1.36E+00
<b>50</b>	9.259	2.198	21.598	5.43E-03	6.733	2.31E-03	3140.598	1.47E+00
<b>51</b>	9.368	2.227	21.600	5.77E-03	6.732	2.55E-03	3141.019	1.58E+00
<b>52</b>	9.197	2.179	21.615	6.00E-03	6.731	2.62E-03	3144.586	1.58E+00
<b>53</b>	9.477	2.246	21.611	5.91E-03	6.733	2.69E-03	3144.621	1.58E+00
<b>54</b>	9.402	2.222	21.656	6.35E-03	6.724	2.43E-03	3153.719	1.58E+00
<b>55</b>	10.324	2.435	21.583	6.65E-03	6.714	2.75E-03	3127.435	1.68E+00
<b>56</b>	10.100	2.392	21.577	5.24E-03	6.741	3.13E-03	3138.377	1.62E+00
<b>57</b>	10.092	2.383	21.550	5.24E-03	6.737	3.43E-03	3128.452	1.63E+00
<b>58</b>	9.792	2.307	21.596	5.04E-03	6.738	3.26E-03	3142.786	1.58E+00
<b>59</b>	5.949	1.473	21.951	2.00E-03	6.820	2.11E-03	3286.171	1.09E+00

#### 4. Additional References

- S1. K. B. Idrees, Z. Li, H. M. Xie, K. O. Kirlikovali, M. Kazem-Rostami, X. J. Wang, X. J. Wang, T. Y. Tai, T. Islamoglu, J. F. Stoddart, R. Q. Snurr and O. K. Farha, Separation of Aromatic Hydrocarbons in Porous Materials, *J Am Chem Soc*, 2022, **144**, 12212-12218.
- S2. C. S. Smoljan, Z. Li, H. Xie, C. J. Setter, K. B. Idrees, F. A. Son, F. Formalik, S. Shafaie, T. Islamoglu, L. K. Macreadie, R. Q. Snurr and O. K. Farha, Engineering Metal-Organic Frameworks for Selective Separation of Hexane Isomers Using 3-Dimensional Linkers, *J Am Chem Soc*, 2023, **145**, 6434-6441.
- S3. K. B. Idrees, K. O. Kirlikovali, C. Setter, H. Xie, H. Brand, B. Lal, F. Sha, C. S. Smoljan, X. Wang, T. Islamoglu, L. K. Macreadie and O. K. Farha, Robust Carborane-Based Metal-Organic Frameworks for Hexane Separation, *J Am Chem Soc*, 2023, **145**, 23433-23441.
- S4. G. Sheldrick, SHELXT: Integrating space group determination and structure solution, *Acta Crystallogr A*, 2014, **70**, C1437-C1437.
- S5. G. M. Sheldrick, SHELXT - Integrated space-group and crystal-structure determination, *Acta Crystallogr A*, 2015, **71**, 3-8.
- S6. G. M. Sheldrick, Crystal structure refinement with SHELXL, *Acta Crystallogr C*, 2015, **71**, 3-8.
- S7. L. R. Redfern, L. Robison, M. C. Wasson, S. Goswami, J. F. Lyu, T. Islamoglu, K. W. Chapman and O. K. Farha, Porosity Dependence of Compression and Lattice Rigidity in Metal-Organic Framework Series, *J Am Chem Soc*, 2019, **141**, 4365-4371.
- S8. L. Robison, X. Y. Gong, A. M. Evans, F. A. Son, X. J. Wang, L. R. Redfern, M. C. Wasson, Z. H. Syed, Z. J. Chen, K. B. Idrees, T. Islamoglu, M. Delferro, W. R. Dichtel, F. X. Coudert, N. C. Gianneschi and O. K. Farha, Transient Catenation in a Zirconium-Based Metal-Organic Framework and Its Effect on Mechanical Stability and Sorption Properties, *J Am Chem Soc*, 2021, **143**, 1503-1512.
- S9. F. A. Son, K. M. Fahy, M. A. Gaidimas, C. S. Smoljan, M. C. Wasson and O. K. Farha, Investigating the mechanical stability of flexible metal-organic frameworks, *Commun Chem*, 2023, **6**, 185.
- S10. R. Hrubiak, S. Sinogeikin, E. Rod and G. Y. Shen, The laser micro-machining system for diamond anvil cell experiments and general precision machining applications at the High Pressure Collaborative Access Team, *Rev Sci Instrum*, 2015, **86**, 072202.
- S11. B. H. Toby and R. B. Von Dreele, GSAS-II: the genesis of a modern open-source all purpose crystallography software package, *J Appl Crystallogr*, 2013, **46**, 544-549.
- S12. T. C. Wang, A. M. Wright, W. J. Hoover, K. J. Stoffel, R. K. Richardson, S. Rodriguez, R. C. Flores, J. P. Siegfried, N. A. Vermeulen, P. E. Fuller, M. H. Weston, O. K. Farha and W. Morris, Surviving Under Pressure: The Role of Solvent, Crystal Size, and Morphology During Pelletization of Metal-Organic Frameworks, *Acs Appl Mater Inter*, 2021, **13**, 52106-52112.
- S13. R. J. Angel, J. Gonzalez-Platas and M. Alvaro, EosFit7c and a Fortran module (library) for equation of state calculations, *Z Krist-Cryst Mater*, 2014, **229**, 405-419.
- S14. J. Gonzalez-Platas, M. Alvaro, F. Nestola and R. Angel, EosFit7-GUI: a new graphical user interface for equation of state calculations, analyses and teaching, *J Appl Crystallogr*, 2016, **49**, 1377-1382.
- S15. E. A. Henle, N. Gantzler, P. K. Thallapally, X. Z. Fern and C. M. Simon, PoreMatMod.jl: Julia Package for in Silico Postsynthetic Modification of Crystal Structure Models, *J Chem Inf Model*, 2022, **62**, 423-432.
- S16. G. Kresse, Ab-Initio Molecular-Dynamics for Liquid-Metals, *J Non-Cryst Solids*, 1995, **193**, 222-229.

- S17. G. Kresse and J. Furthmuller, Efficiency of ab-initio total energy calculations for metals and semiconductors using a plane-wave basis set, *Comp Mater Sci*, 1996, **6**, 15-50.
- S18. G. Kresse and D. Joubert, From ultrasoft pseudopotentials to the projector augmented-wave method, *Phys Rev B*, 1999, **59**, 1758-1775.
- S19. S. Grimme, J. Antony, S. Ehrlich and H. Krieg, A consistent and accurate ab initio parametrization of density functional dispersion correction (DFT-D) for the 94 elements H-Pu, *J Chem Phys*, 2010, **132**, 154104.
- S20. S. Grimme, S. Ehrlich and L. Goerigk, Effect of the damping function in dispersion corrected density functional theory, *J Comput Chem*, 2011, **32**, 1456-1465.
- S21. J. P. Perdew, K. Burke and M. Ernzerhof, Generalized gradient approximation made simple, *Phys Rev Lett*, 1996, **77**, 3865-3868.
- S22. G. Kresse and J. Furthmuller, Efficient iterative schemes for ab initio total-energy calculations using a plane-wave basis set, *Phys Rev B*, 1996, **54**, 11169-11186.
- S23. D. E. P. Vanpoucke, J. W. Jaeken, S. De Baerdemacker, K. Lejaeghere and V. Van Speybroeck, Quasi-1D physics in metal-organic frameworks: MIL-47(V) from first principles, *Beilstein J Nanotech*, 2014, **5**, 1738-1748.
- S24. A. S. Rosen, J. M. Notestein and R. Q. Snurr, Comparing GGA, GGA+U, and meta-GGA functionals for redox-dependent binding at open metal sites in metal-organic frameworks, *J Chem Phys*, 2020, **152**, 224101.
- S25. J. F. Nye, *Physical Properties of Crystals*, Oxford University Press, 1957.
- S26. R. Yu, J. Zhu and H. Q. Ye, Calculations of single-crystal elastic constants made simple, *Comput Phys Commun*, 2010, **181**, 671-675.
- S27. M. de Jong, W. Chen, T. Angsten, A. Jain, R. Notestine, A. Gamst, M. Sluiter, C. K. Ande, S. van der Zwaag, J. J. Plata, C. Toher, S. Curtarolo, G. Ceder, K. A. Persson and M. Asta, Charting the complete elastic properties of inorganic crystalline compounds, *Sci Data*, 2015, **2**.
- S28. R. Gaillac, P. Pullumbi and F. X. Coudert, ELATE: an open-source online application for analysis and visualization of elastic tensors, *J Phys-Condens Mat*, 2016, **28**, 275201.
- S29. Z. Li, K. H. Shi, D. Dubbeldam, M. Dewing, C. Knight, A. Vázquez-Mayagoitia and R. Q. Snurr, Efficient Implementation of Monte Carlo Algorithms on Graphical Processing Units for Simulation of Adsorption in Porous Materials, *J Chem Theory Comput*, 2024, **20**, 10649-10666.
- S30. S. L. Mayo, B. D. Olafson and W. I. I. I. Goddard, Dreiding - a Generic Force-Field for Molecular Simulations, *J Phys Chem-U*s, 1990, **94**, 8897-8909.
- S31. M. Dinpajoooh, P. Bai, D. A. Allan and J. I. Siepmann, Accurate and precise determination of critical properties from Gibbs ensemble Monte Carlo simulations, *J Chem Phys*, 2015, **143**.
- S32. F. Hund and K. Lieck, Das Quinare Fluorid Nacacdyf8, *Z Anorg Allg Chem*, 1952, **271**, 17-28.
- S33. J. P. S. Mowat, V. R. Seymour, J. M. Griffin, S. P. Thompson, A. M. Z. Slawin, D. Fairen-Jimenez, T. Duren, S. E. Ashbrook and P. A. Wright, A novel structural form of MIL-53 observed for the scandium analogue and its response to temperature variation and CO<sub>2</sub> adsorption, *Dalton T*, 2012, **41**, 3937-3941.
- S34. J. H. Lee, A. Jaffe, Y. Lin, H. I. Karunadasa and J. B. Neaton, Origins of the Pressure-Induced Phase Transition and Metallization in the Halide Perovskite (CH<sub>3</sub>NH<sub>3</sub>)PbI<sub>3</sub>, *Acs Energy Lett*, 2020, **5**, 2174-2181.
- S35. F. Formalik, A. V. Neimark, J. Rogacka, L. Firlej and B. Kuchta, Pore opening and breathing transitions in metal-organic frameworks: Coupling adsorption and deformation, *J Colloid Interf Sci*, 2020, **578**, 77-88.

- S36. A. E. J. Hoffman, J. Wieme, S. M. J. Rogge, L. Vanduyfhuys and V. Van Speybroeck, The impact of lattice vibrations on the macroscopic breathing behavior of MIL-53(Al), *Z Krist-Cryst Mater*, 2019, **234**, 529-545.